Available online at www.ijournalse.org

Emerging Science Journal

(ISSN: 2610-9182)

Vol. 10, No. 1, February, 2026

Multi-Country GHG Emissions Forecasting by Sector Using a GCN-LSTM Model

Babey Dimla Tonny [1], Krisanadej Jaroensutasinee [1*], Mullica Jaroensutasinee [1], Elena B. Sparrow [2]

[1] *Center of Excellence for Ecoinformatics, School of Science, Walailak University, Nakhon Si Thammarat, Thailand.*

[2] *Department of Natural Resources and Environment, University of Alaska Fairbanks, AK, United States.*

Abstract

This study developed a novel hybrid Graph Convolutional Network–Long Short-Term Memory (GCN–LSTM) model to forecast greenhouse gas (GHG) emissions across multiple country sectors, aiming to enhance climate policy. We analyzed 52 years (1970–2022) of GHG emissions data (CO_2 , CH_4 , N_2 O, F-Gases) from 163 countries and eight sectors (Agriculture, Buildings, Fuel Exploitation, Industrial Combustion, Power Industry, Processes, Transport, Waste), sourced from the EDGAR v8 database. The GCN adjacency matrix captures spatial relationships on a weighted sum of Haversine distance and cosine similarity, while the LSTM models temporal dynamics. Data preprocessing includes min-max scaling and outlier handling with Interquartile Range capping. The model was trained on 70% of the data, validated on 15%, and tested on 15%, using Mean Squared Error (MSE) loss and the Adam optimizer. The performance was evaluated with Mean Absolute Error (MAE), Root Mean Squared Error (RMSE), and Coefficient of Determination (R^2). The GCN–LSTM model outperformed baseline models (ARIMA, Simple LSTM, Stacked LSTM), achieving the lowest MAE (0.0207 in Waste) and highest R^2 (0.9756 in Waste). Model interpretability highlighted strong regional connections, such as Thailand–Cambodia in the Waste sector, suggesting that spatial and temporal dependencies offer superior forecasting accuracy, informing targeted climate action.

Keywords:

Graph Convolutional Networks;
Long Short-Term Memory;
Greenhouse Gas Emissions;
Climate Policy; Model Interpretability;
Forecasting Accuracy.

Article History:

Received:	02	July	2025
Revised:	03	December	2025
Accepted:	21	December	2025
Published:	01	February	2026

1- Introduction

Accurate forecasting of greenhouse gas (GHG) emissions has, in the past, proven to be a critical contributor to developing effective climate policies and achieving global sustainability goals. Rising emissions, predominantly from anthropogenic sources of carbon dioxide (CO_2), methane (CH_4), nitrous oxide (N_2O), and fluorinated gases (F-gases), pose significant challenges to mitigating climate change. For instance, global CO_2 emissions reached a record high in 2022, rebounding sharply from a temporary decline during the COVID-19 pandemic [1, 2]. CH_4 concentrations have shown a renewed increase since 2007, with notable acceleration between 2014 and 2017 [3, 4], while N_2O emissions have risen by 30% over the past four decades, primarily driven by human activity [5]. F-gas emissions are also increasing, particularly in developing countries, necessitating urgent attention [6].

Exploratory data analysis from Table 1 and Figure 1 reveals that CO_2 exhibits a mean normalized emission of 0.003151 and a variance of 0.000424, indicating its significant presence and variability. CH_4 and F-gases show higher means (0.006341 and 0.007880, respectively) and variances, suggesting their substantial contributions to rising

* **CONTACT**: krisanadej@gmail.com; jkrisana@wu.ac.th

DOI: http://dx.doi.org/10.28991/ESJ-2026-010-01-03

emissions. All GHGs display high skewness, particularly CO_2 (20.530403) and N_2O (18.939121), pointing to the presence of high-emission outliers and a tendency for growing emission events [7]. These indicators underscore the need for robust forecasting models that can capture complex emission patterns across multiple countries and sectors to inform targeted policy interventions.

Table 1. Mean, variance, and skewness for GHG emissions distribution for substances: (a) CO_2, (b) CH_4, (c) N_2O, and (d) F-Gases (EDGAR data Appendix A)

	CO_2	CH_4	N_2O	F-Gases
Mean	0.003151	0.00634	0.004203	0.007880
Variance	0.000424	0.001271	0.000813	0.001836
Skewness	20.530403	13.310114	18.939121	13.073908

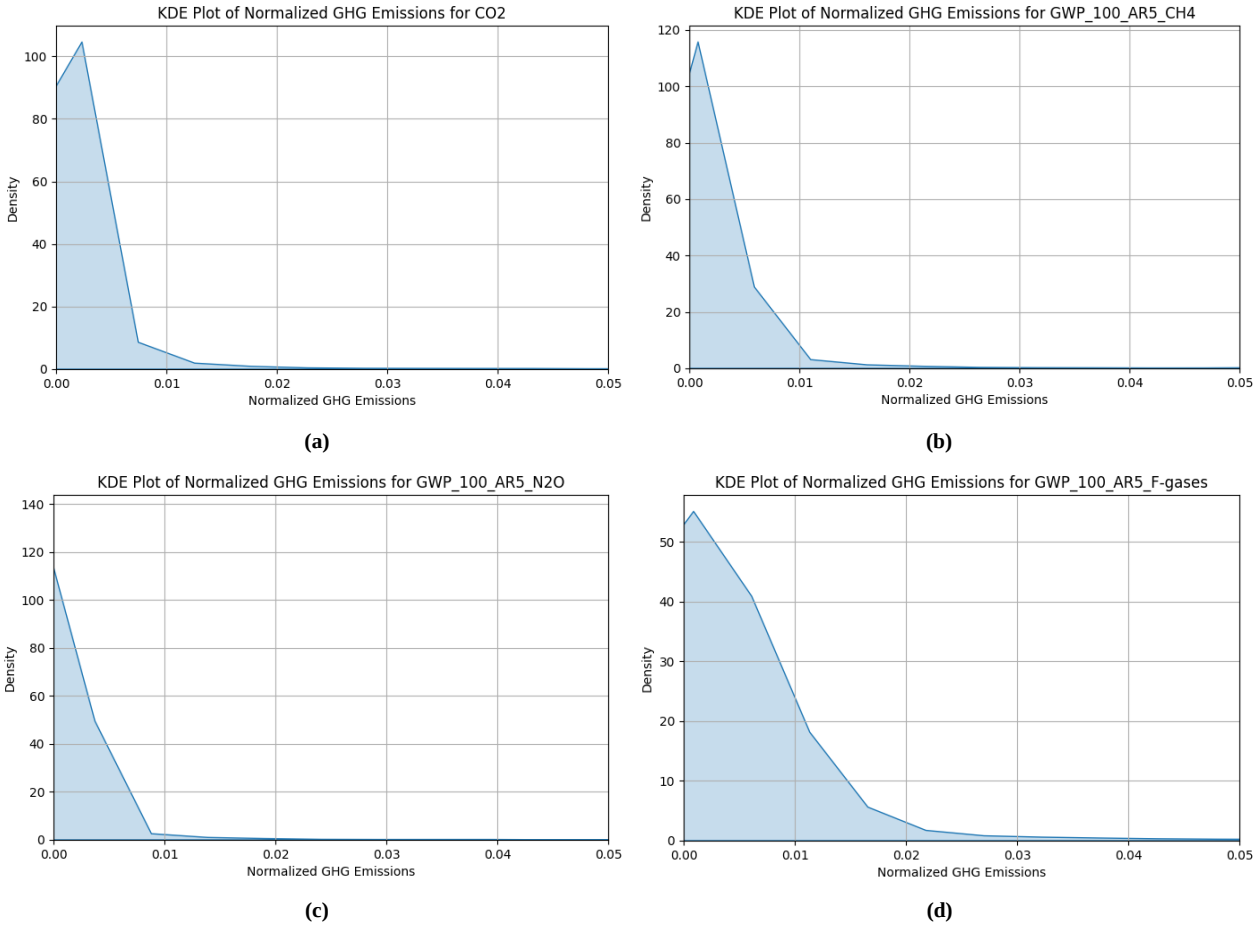

Figure 1. Kernel Density plot of GHG emissions distribution for substances: (a) CO_2, (b) CH_4, (c) N_2O, and (d) F-Gases (EDGAR data Appendix A)

In recent decades, GHG emissions forecasting has evolved significantly with advancements in data analysis and numerical computation. Traditional statistical models, developed to advance science in this domain, such as Autoregressive Integrated Moving Average (ARIMA), have been widely used with appreciable success, yet are marred with challenges, such as the inability to capture non-linear relationships inherent in emissions data [8, 9]. Such limitations drove researchers to invent machine learning (ML) models to improve forecasting accuracy, with methods like decision trees and support vector machines outperforming traditional approaches [10, 11]. In a world in dire need of the best possible tools to solve climate change, scientists have continually sought after even more robust instruments to resolve this problem. This has led to the development of even more advanced ML models such as advanced deep learning models, notably, Long Short-Term Memory (LSTM) neural networks [3], a variant of Recurrent Neural Networks that excel at capturing temporal trends in time-series data [12, 13] and has been demonstrated in a vast and diverse array of applications like air temperature forecasting [14], solar radiation [15] and CO_2 emissions prediction [16, 17]. Despite the prolificity of LSTMs, these models are limited in their ability to account for spatial interactions between

proximate geographic locations with potential for inter-location spill-over emissions, a critical piece of information needed for understanding global emissions dynamics influenced by economic, geographic, and policy-related factors [18, 19].

To address this limitation of LSTMs, researchers have developed and applied hybrid models that integrate the strengths of spatial modeling to complement the robust temporal modeling ability of LSTMs. In the domain of spatial modeling, models like Convolutional Neural Networks (CNN) have been broadly used [20]. CNNs, although prolific, are fundamentally designed to handle structured grid data. This has limited their ability to model the often-unstructured spatial distribution of emission sources, a challenge that is addressed by another model called Graph Neural Networks (GNN) [21]. A popular variant of GNNs, the Graph Convolutional Networks (GCNs) models spatial relationships by notating data as graphs [22], making them suitable for capturing interactions between countries or regions [23, 24] with potential cross-border emissions. Recent research has explored the combination of GCNs with LSTMs, which has proven to be effective in domains such as power load forecasting [25], transportation [26], and air quality prediction [27]. For instance, Shao et al. [7] proposed a hybrid spatiotemporal GCN model for multiregional carbon emissions forecasting, highlighting its ability to integrate spatial dependencies. Similarly, García-Duarte et al. [18] applied GCNs to spatial-temporal air temperature forecasting, demonstrating their potential for environmental applications. Despite these advances, there remains a critical gap in the application of hybrid GCN-LSTM models to multi-country, sector-specific GHG emissions forecasting, which is essential for developing granular and actionable climate policies across diverse regions and industries [7, 11].

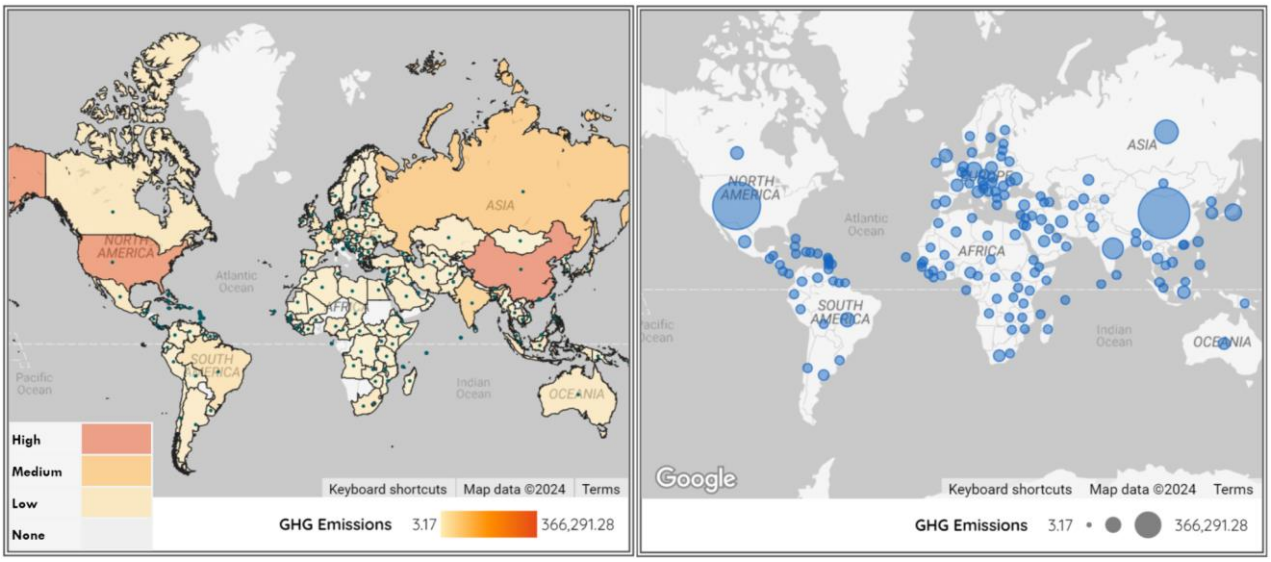

(a) **(b)**

Figure 2. (a) Color Map and (b) Bubble Map of 163 countries [Appendix A] displaying the amount of Greenhouse gas emissions from lowest through medium to highest in $MtCO_2e$

This study addresses this gap by developing a novel GCN-LSTM hybrid model for forecasting GHG emissions across 163 countries and eight sectors (Figure 2, Appendix A), utilizing a comprehensive 52-year dataset from the Emissions Database for Global Atmospheric Research (EDGAR). The model leverages GCNs to capture spatial relationships, such as geographic proximities and emissions similarities between countries, and LSTMs to model temporal trends, incorporating node features like total GHG emissions and GHG per capita to analyze both macro-level and micro-level patterns [28]. The key contributions from this study include: (1) a sophisticated data preprocessing pipeline with node feature engineering and dynamic graph construction; (2) a novel GCN-LSTM architecture for spatial-temporal feature extraction; (3) a spatial interpretability analysis of the GCN adjacency matrix, using Southeast Asia as a case study to provide actionable insights into regional emission patterns; (4) comprehensive performance evaluation against baseline models (ARIMA, simple LSTM, and stacked LSTM) using metrics such as Mean Absolute Error (MAE), Root Mean Squared Error (RMSE), and Coefficient of Determination (R^2), supplemented by paired *t*-tests across all sectors (p-value < 0.05), reported in Appendix B); (5) 5-fold cross-validation to ensure model robustness; and (6) interpretable insights into emission trend drivers to support targeted climate policies [7, 29]. To advance environmental informatics, this study provides a robust tool for emissions forecasting, enabling policymakers to address global, regional, and sectoral climate challenges effectively.

The paper is organized as follows: Section 2 describes the data sources, preprocessing pipeline, and details of the GCN-LSTM model architecture and methodology. Section 3 presents the experimental results, comparisons with the baseline model, and figurative interpretability. Section 4 discusses the implications of the findings and suggests directions for future research, while Section 5 presents the study's conclusion.

2- Materials and Methods

2-1- Theoretical Approach

The theoretical framework of the novel hybrid Graph Convolutional Network–Long Short-Term Memory (GCN-LSTM) model proposed in this study is grounded in spatial-temporal data modeling. This approach integrates graph-based spatial dependencies with time-series analysis. GCNs leverage graph theory to model relationships between entities (countries in this case), which are referred to as nodes, connected by relationships referred to as edges. The edge connections are defined here by an adjacency matrix constructed from a weighted sum of Haversine distance and cosine similarity of emission profiles [18]. This approach is designed to enable the model to capture spatial interactions, such as shared emission patterns and spill-over effects due to geographic proximity or policy similarities, theoretically supported by studies on spatial econometrics [27]. The LSTM component, rooted in Recurrent Neural Network (RNN) theory, models temporal dependencies in the GHG time-series data by maintaining memory cells that capture long-term trends in greenhouse gas (GHG) emissions [16]. This fusion of GCN and LSTM empowers the model to learn both spatial correlations (e.g., regional emission clusters) and temporal dynamics (e.g., emission trends over 1970–2022), addressing limitations of traditional models like ARIMA and independent LSTMs, which lack spatial awareness [30]. This theoretical synergy enhances forecasting accuracy and interpretability, putting forward a robust framework for multi-country, sector-specific GHG analysis to support climate policy design [31].

2-2- Technical Implementation

Building on the theoretical framework of spatial-temporal modeling outlined in section 2-1, this section describes the technical implementation of the Graph Convolutional Network–Long Short-Term Memory (GCN-LSTM) model for forecasting greenhouse gas (GHG) emissions across 163 countries and eight sectors (Appendix A) using the EDGAR v8 dataset (1970–2022). The implementation, illustrated in Figure 3, encompasses data preprocessing, model architecture, training, and validation.

- **Data Preprocessing:** The collected EDGAR v8 data consisted of 213 countries, including global shipping and aviation. The data were filtered to exclude countries with missing or incomplete records, retaining 163 countries with complete records (GHG emissions, substance, sector, year, and GHG per Capita), requiring no data imputation. It was then preprocessed to handle outliers using the Interquartile Range (IQR) method, capping values at 1.5 × IQR bounds [32]; normalized with min-max scaling, and the features extracted for modeling. The adjacency matrix was constructed using a weighted sum of Haversine distance and cosine similarity, with a 2,000 km distance threshold and 0.01 edge strength (Appendix C). The distance threshold of 2,000 km was a rounded-up value determined as an approximate average Haversine distance (~1813 km) calculated from pairwise distances among 11 Southeast Asian capitals (Brunei Darussalam, Cambodia, Indonesia, Laos, Myanmar, Malaysia, Philippines, Singapore, Thailand, Timor-Leste, Vietnam), totaling 99,697 km across 55 unique pairs (Appendix C-1). The edge strength threshold of 0.01 was empirically selected by visualizing adjacency matrix connections in the GCN, where meaningful regional clusters (Appendix A) emerged at this threshold, as observed in a graph plot with connection strengths ranging from 0.001 to 0.02 (Appendix C-2).

- **Model Architecture:** The GCN-LSTM model integrates a GCN layer (64 hidden units) to capture spatial dependencies and an LSTM layer (64 hidden units) for temporal dynamics (as detailed in Table 3, section 2-1) [16]. The model was trained with a learning rate of 0.001 and batch sizes alternating between 16 and 32 for best performance by sector and optimized using 5-fold cross-validation to minimize validation loss, ensuring robust hyperparameter selection [27].

- **Validation:** Model performance was evaluated using Mean Absolute Error (MAE), Root Mean Squared Error (RMSE), and Coefficient of Determination (R^2) on a test set (2016–2022). Paired *t*-tests were used to confirm statistically significant improvements ($p < 0.05$) of GCN-LSTM over baseline ARIMA (Appendix B) across all sectors, validating its superior accuracy [30]. The flow diagram (Figure 3) illustrates the data pipeline, model training, and validation process, detailed in Section 4.

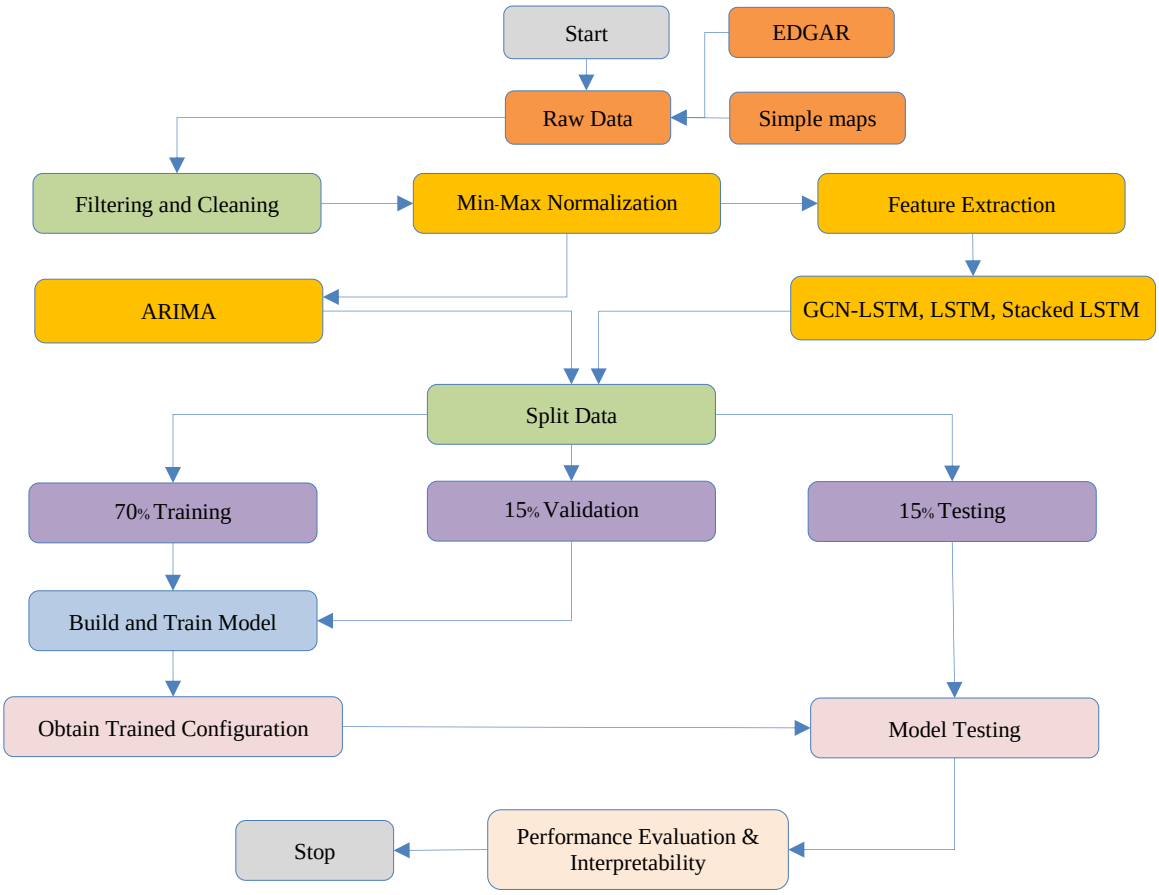

Figure 3. Diagrammatic Representation of Implementation Methodology

The computing device specifications and estimated inference runtimes are presented in Table 2.

Table 2. Specifications of the computing device and run times

Specification	Value	Model	Estimated Run Times (Seconds)
Operating System	Windows 11 Pro 64-bit (10.0, Build 26100)	GCN-LSTM	30 - 60
System Model	Precision 5530	Simple LSTM	10 - 45
Memory	32GB RAM	Stacked LSTM	20 - 60
Processor	Intel Core i9-8950 HK @ 2.9GHz (12 threads, up to 4.8GHz)	ARIMA	5 - 30
Graphics	NVIDIA Quadro P2000 (4GB dedicated, 20.277GB total)		

2-3- Data Preprocessing

(a) Data Filtering

The primary dataset spans 213 countries and unique regions, including international shipping and aviation. This data includes emissions data for four substances (CO_2 , CH_4 , N_2 O, and F-Gases) across eight sectors (Agriculture, Buildings, Fuel Exploitation, Industrial Combustion, Power Industry, Processes, Transport, and Waste) and spans the period from 1970 to 2022. To ensure data consistency and quality, we filtered the dataset to retain only countries with complete records for substance, sector, year, GHG emissions, and GHG per capita. This results in a final dataset of 163 countries, with a brief explanation of the dataset provided in [Appendix A].

(b) Aggregation of Emissions by Sector

Noting that we were forecasting total emissions by sector, we aggregated emissions measured in megatons of carbon dioxide equivalent ($MtCO_2e$) from all four substances into their respective industries. For each Country i, Sector k and Year, t, the total Emissions $E_{i,k,t}$ are computed as the summation of emissions across all Substances j (CO_2, CH_4, N_2O, F-Gases):

$$E_{i,k,t} = \sum E_{i,j,k,t} \quad (1)$$

where, $E_{i,j,k,t}$ represents emissions for Country i, Substance $j$and Sector k in the Year t. and $E_{i,k,t}$ represents the total emissions for Country i, and Sector k in Year t.

This aggregation step ensured that the emissions data were sector-specific and comparable across countries and years. The resulting dataset contains total emissions and GHG per capita for each of the eight sectors in 163 countries.

(c) Outlier Handling

Outliers for each country sector were identified and capped using the Interquartile Range (IQR) method [31]. For a given column x, the IQR is calculated as:

$$IQR = Q_3 - Q_1 \tag{2}$$

where, $Q_1 \in [0, 25]$ is the 25th percentile and $Q_3 \in [75, 100]$ is the 75th percentile. Values outside these bounds are capped to the nearest bounds defined as:

$$\begin{aligned} Lower\ Bound &= Q_1 - 1.5 \times IQR, \\ Upper\ Bound &= Q_3 - 1.5 \times IQR \end{aligned} \tag{3}$$

The IQR bounds varied across sectors, with Agriculture, Fuel Exploitation, and Waste sharing the widest range, from 0 to 95. The Power Industry was set at a range of 0 to 94, while Transport ranged from 0 to 90, Processes from 0 to 80, Industrial Combustion from 0 to 75, and Buildings, a more constrained IQR, ranged from 15 to 85.

(d) Normalization

To facilitate the practical training of the GCN-LSTM model, we normalized emissions and GHG per capita values for each feature *f*, using the Min-Max scaling method, ensuring consistent data scales. This normalization step ensured that all features were scaled to the range of [0, 1]. For each country, sector, and year, the normalized value $\hat{f}$ is calculated as:

$$\hat{f} = \frac{f - min(f)}{max(f) - min(f)} \tag{4}$$

where; $min(f)$ and $max(f)$ are the minimum and maximum values of features f for each country, sector, and year.

2-4- Model Architecture

The hybrid model processed graph-structured data with two GCN layers to extract spatial features, modeled temporal dependencies with an LSTM layer, and generated final predictions with two fully connected layers (Figure 4).

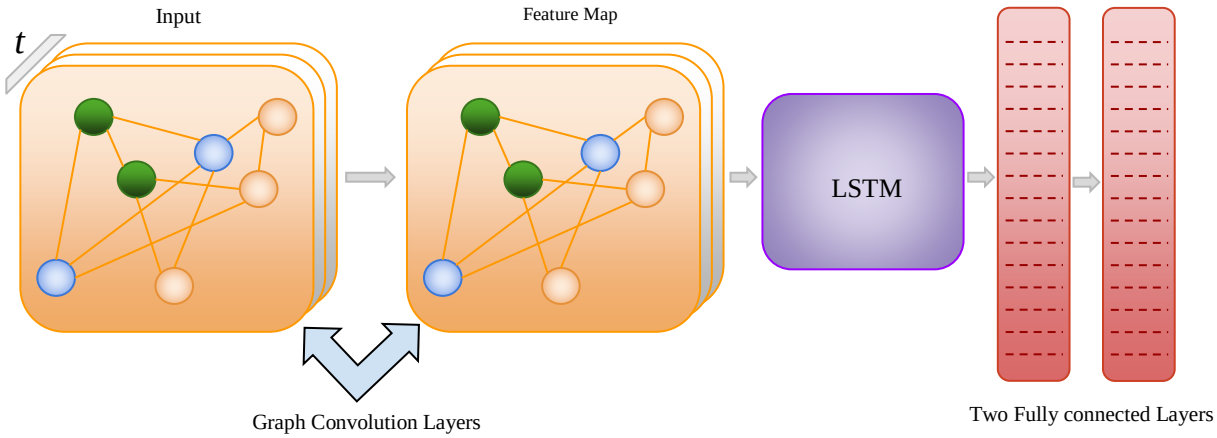

Figure 4. Basic Architecture of the GCN-LSTM Model

(a) GCN Component

The GCN processed updates between layers such that for each layer l, the node features $H^{(l)}$ are updated as:

$$H^{(l+1)} = \sigma(\hat{D}^{-\frac{1}{2}}\hat{A}\hat{D}^{-\frac{1}{2}}H^{(l)}W^{(l)}) \tag{5}$$

where, $\hat{A}$ is the adjacency matrix with added self-connections; $\hat{D}$ is the diagonal degree matrix of $\hat{A}$; $W^{(l)}$ is the weight matrix for the layer l; and σ is a non-linear activation function ReLU.

(b) Graph Construction

We used the preprocessed dataset to construct a graph representing the spatial relationships between countries, where countries served as nodes and edges were defined by geographic proximity and emissions similarity [32]. Each node in the graph was associated with two key features: Total GHG emissions and GHG per capita. These features were used as

input to the GCN component of the hybrid model. On the other hand, edges were defined by the Adjacency matrix, constructed based on a weighted sum of an exponentially decaying Haversine distance with a threshold of 2,000 km (using latitudes and longitudes for each country) and cosine similarity. The resultant connection strength was set to a threshold of 0.01 and captured for interpretability analysis.

The **Haversine distance** d_{i_1,i_2} between two countries i_1 *and* i_2 was calculated as:

$$d_{i_1,i_2} = 2\,Arcsin(\sqrt{sin^2(\frac{\Delta lat}{2}) + cos(lat_{i_1})cos(lat_{i_2})sin^2(\frac{\Delta lon}{2})}) \tag{6}$$

where, R is the Earth's radius; and Δlat and Δlon are the differences in latitude and longitude between countries i_1 and i_2.

The **cosine similarity** s_{i_1,i_2} between the emission vectors of countries i_1 and i_2 is calculated as:

$$s_{i_1,i_2} = \frac{e_{i_1}.\ e_{i_2}}{||e_{i_1}||\,||e_{i_2}||} \tag{7}$$

where, e_{i_1} and e_{i_2} are the emission vectors of countries i_1 and i_2 , respectively.

The resultant Adjacency matrix A is defined as:

$$A_{i_1,i_2} = exp(-\frac{d_{i_1,i_2}}{\sigma d}) + \alpha s_{i_1,i_2} \tag{8}$$

Where, σd is the scaling factor for distance; and αs is a weight parameter for the cosine similarity.

This graph construction process ensured that the GCN component of the model effectively captured the spatial relationships between countries.

(c) LSTM Component

The LSTM component processed the temporal sequence of the emissions data (Figure 5). For each time step t, the LSTM cell updated its hidden state h_t and cell state c_t as:

$$\begin{aligned} f_t &= \sigma(W_f[Z, h_{t-1}] + b_f) \\ i_t &= \sigma(W_i[Z, h_{t-1}] + b_i) \\ o_t &= \sigma(W_o[Z, h_{t-1}] + b_o) \\ \underline{c_t} &= tanh(W_c[Z, h_{t-1}] + b_c) \\ c_t &= f_t \odot c_{t-1} + i_t \odot \underline{c_t} \\ h_t &= o_t \odot tanh(c_t) \end{aligned} \tag{9}$$

Where, Z, The node embedding output from the GCN serves as input to the LSTM; f_t , i_t and o_t are the forget, input, and output gates, respectively; W and b are the weight matrices and bias vectors; σ and $tanh$ are the neural network activation functions; and $\odot$ Denotes pointwise multiplication.

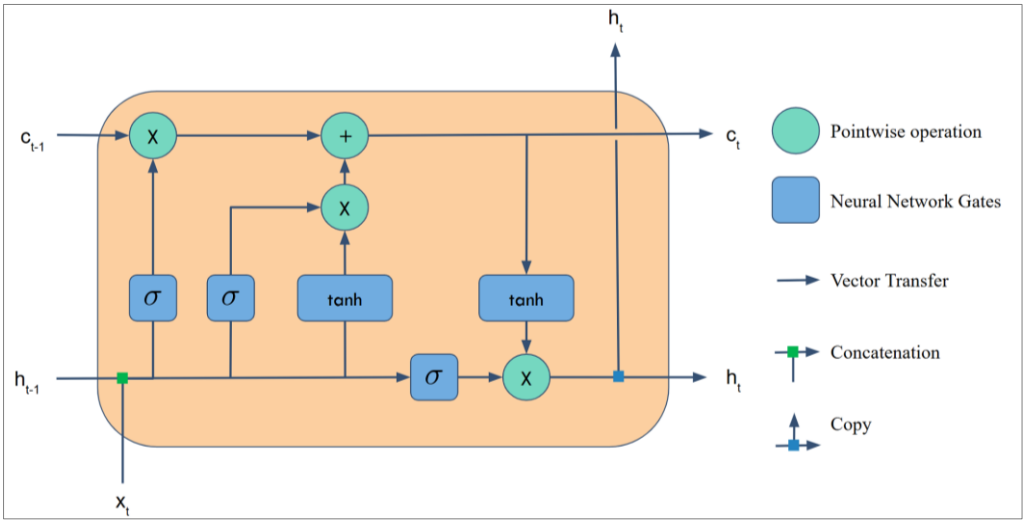

Figure 5. LSTM Cell Structure

(d) Attention Mechanism

The attention mechanism computed a weighted sum of LSTM hidden states, dynamically learning the weights from the input data, to focus the model on relevant temporal features. In this study, we implemented the attention mechanism in Python code using the Multi-Head-Attention layer from TensorFlow. The attention operation can be expressed as:

$$Attention\ (Q, K, V)\ =\ softmax(\frac{QK^T}{\sqrt{d_K}})V \tag{10}$$

where, $Q, K,$ and V are the query, key, and value matrices, respectively; and d_K is the dimensionality of the key vectors.

2-5- Training and Evaluation

(a) Data Splitting

We randomly split the preprocessed dataset for each country sector into 70% training, 15% validation, and 15% testing, preserving the temporal order. We then sorted the data chronologically by year to ensure temporal consistency and evaluated the model on unseen future data.

(b) Model Training

For ARIMA, we applied a uniform Autoregressive (1), Integrated (1), and Moving Average (1) configuration model with a sequence length of one (1) across all sectors. We trained deep learning models with the Adam optimizer and MSE loss, optimizing parameters per country sector. We used early stopping (patience 10, max 100 epochs) to prevent overfitting. Hyperparameters were selected through sensitivity analysis, considering only hyperparameters with a significant observable influence on the evaluation metrics for each sector, and are listed in Table 3.

Table 3. Optimal GCN-LSTM, Simple LSTM, and Stacked LSTM Hyperparameters

Sector	Sequence Length	Threshold Distance (GCN-LSTM only)	Batch Size	Hidden Size	Number of Layers	Epochs/Patience
Agriculture	6	2000	16	64	2 GCN + 1 LSTM	100/10
Buildings	1	2000	32	64	2 GCN + 1 LSTM	100/10
Fuel Exploitation	1	2000	16	64	2 GCN + 1 LSTM	100/10
Industrial Combustion	2	2000	16	64	2 GCN + 1 LSTM	100/10
Power Industry	1	2000	16	64	2 GCN + 1 LSTM	100/10
Processes	1	2000	16	64	2 GCN + 1 LSTM	100/10
Transport	6	2000	32	64	2 GCN + 1 LSTM	100/10
Waste	6	2000	32	64	2 GCN + 1 LSTM	100/10

(c) Model Evaluation Metrics

We evaluated the trained GCN-LSTM model using standard regression metrics, including:

1. **Mean Absolute Error (MAE)**: MAE calculates the average absolute difference between predicted and actual emissions, expressed in megatons of CO_2 equivalent (Mt CO_2e).

$$MAE = \frac{1}{N}\sum |E_{i,k,t} - \hat{E}_{i,k,t}| \tag{11}$$

2. **Root Mean Squared Error (RMSE):** RMSE measures the square root of the average squared difference between predicted and actual values. It's more sensitive to significant errors than MAE, which makes it worthwhile when significant errors are undesirable.

$$RMSE = \sqrt{\frac{1}{N}\sum (E_{i,k,t} - \hat{E}_{i,k,t})^2} \tag{12}$$

3. **Coefficient of Determination (R^2):** R^2, which ranges from 0 to 1, measures the predictive accuracy by explaining the variance in actual emissions. A value of 1 indicates perfect predictions.

$$R^2\ = 1 - \frac{\sum E_{i,k,t} - \hat{E}_{i,k,t}}{\sum E_{i,k,t} - \underline{E}_{i,k,t}} \tag{13}$$

Where for all three equations above: $E_{i,k,t}$ represents actual emissions for the Country i, and Sector k in Year t; $\hat{E}_{i,k,t}$ represents predicted emissions for the Country i, and Sector k in Year t; and $\underline{E}_{i,k,t}$ represents the mean of the actual emissions for Country i, and Sector k in Year t.

2-6- Methodology for Model Interpretability

We performed an interpretability analysis to understand and validate the model's predictions. In this study, we characterized the interpretability of the GCN-LSTM model in regional-only, regional-temporal, and spatial analyses to dissect its performance across all eight sectors [Appendix A]. The spatial connections, filtered at a threshold connection strength of 0.01 were represented in variations of strength (Figure 8) differentiated by line color and thickness: dark blue (<0.0156), sky blue (0.0156–0.0194), orange (0.0194–0.0232), and dark red (>0.0232) as shown in Section 3(c). This approach provides insights into its behavior across different geographical regions, both spatially and over time. For both regional-only and regional-temporal analysis, we grouped countries into predefined regional clusters [Appendix A] and analyzed the performance metrics for each region and sector. We calculated the MAE, RMSE, and R^2 to evaluate the model's performance. Regions were then categorized into three levels (Level 1 Regions: Best performance within each sector; Level 2 Regions: Performance just below Level 1; and Level 3 Regions: Performance below Level 2) as shown in Table 4 and Table 5. The overall model performance is then evaluated with the metrics in Table 6 and Figure 10.

3- Results

3-1- GCN-LSTM Model Interpretability

Figure 6 evaluates the GCN-LSTM model's performance across eight sectors (Appendix A) using Mean Absolute Error (MAE) in $MtCO_2e$, as detailed in Table 4 (Section 3- 1a, Regional Interpretability). The vertical axis represents MAE, while the horizontal axis lists regions categorized into the three performance levels (Level 1: best, Level 2: moderate, Level 3: lower) mentioned in sections 2-6 and based on clusters in Appendix A. For example, Southeast Asia's Waste sector achieves Level 1 with an MAE of 0.0207, reflecting high accuracy due to strong spatial connections (see Figure 8). This demonstrates the GCN-LSTM's ability to leverage spatial relationships, captured through its graph-based architecture, to improve emission forecasts. Level 1 performance in these interconnected regions highlights the model's robustness in handling data influenced by geographic proximity, making it a reliable tool for cross-sectoral and cross-regional analysis.

(a) Regional Interpretability

Table 4. Region-Only Performance Evaluation by MAE, RMSE, and R^2 Levels

Sector	Range MAE	Range RMSE	Range R^2	Level 1 Regions	Level 2 Regions	Level 3 Regions
Agriculture	0.045-0.063	0.259-0.311	0.903-0.953	Caribbean, Southern Cone	Micronesia, Northern South America	Brazil, Central Africa
Buildings	0.050-0.072	0.269-0.347	0.875-0.953	Micronesia, Caribbean	Northern Europe, Polynesia	Southern Cone, West Asia
Fuel Exploitation	0.043-0.058	0.272-0.360	0.850-0.954	Southern Africa, Central Africa	Polynesia, North Africa	West Asia, Northern Europe
Industrial Combustion	0.044-0.075	0.247-0.376	0.812-0.970	Brazil, Micronesia	Caribbean, Central America	Southern Cone, North America
Power Industry	0.041-0.058	0.249-0.305	0.917-0.961	Polynesia, Northern Europe	North America, Andean Countries	Southern Europe, West Africa
Processes	0.039-0.057	0.258-0.373	0.826-0.962	Caribbean, Eastern Europe	West Asia, South Asia	Southern Cone, Northern Europe
Transport	0.038-0.054	0.246-0.303	0.902-0.962	North America, Central Asia	Southern Europe, Micronesia	West Africa, Andean Countries
Waste	0.015-0.027	0.145-0.267	0.942-0.995	Micronesia, Southern Cone	Polynesia, East Asia	Central Africa, West Africa

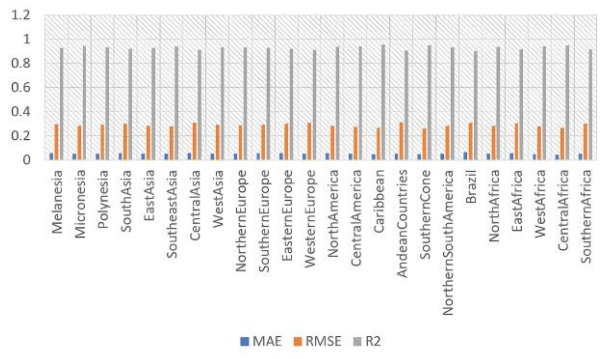

(a) Agriculture

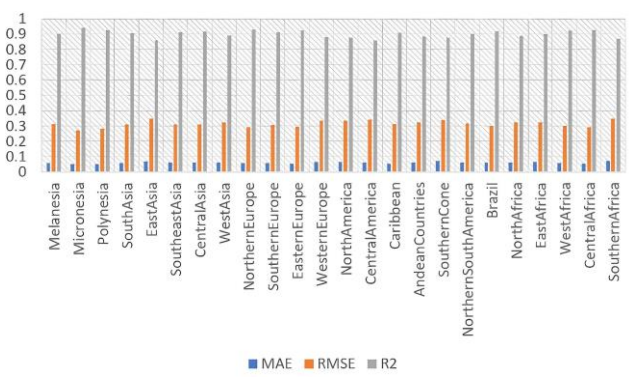

(b) Buildings

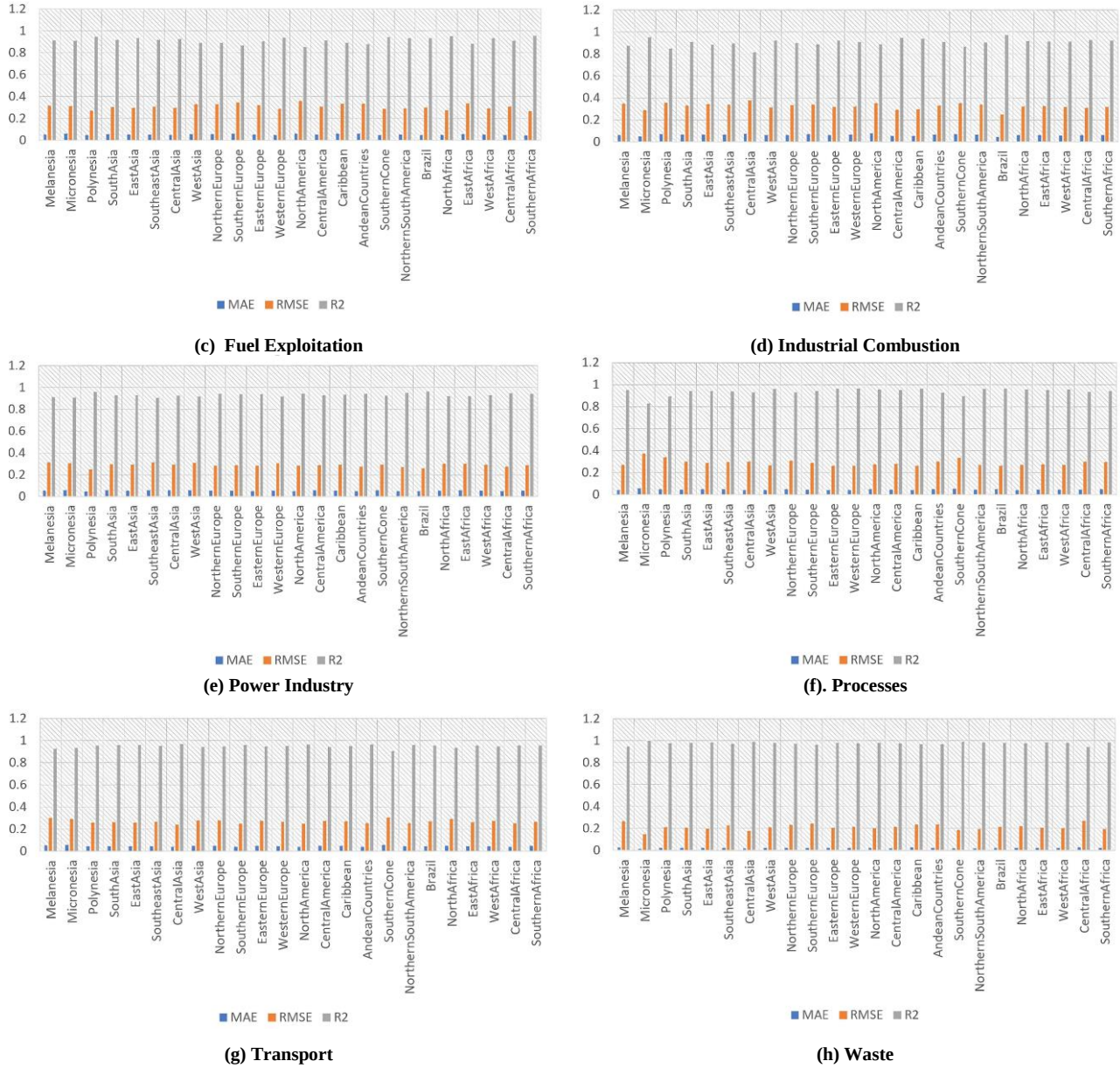

(c) Fuel Exploitation

(d) Industrial Combustion

(e) Power Industry

(f). Processes

(g) Transport

(h) Waste

Figure 6. Regional evaluation for all eight sectors: (a), (b), (c), (d), (e), (f), (g), (h). Blue, orange, and gray bars represent MAE, RMSE in $MtCO_2e$, and R^2, respectively

(b) Temporal Interpretability

Building on Figure 6, Figure 7 tracks the temporal evolution of MAE for the GCN-LSTM model across the same sectors and regional clusters over 1970–2022, as summarized in Table 5 (Section 3-1b, Temporal Interpretability). The vertical axis shows MAE (in $MtCO_2e$). In contrast, the horizontal axis denotes regions for Figure 7(a) and years for Figure 7(b), with lines color-coded by sector (e.g., Waste: brown, Agriculture: green). Southeast Asia's Waste sector, for instance, shows a MAE decline from 0.045 $MtCO_2e$ in the 1970s to 0.0207 $MtCO_2e$ by 2022, indicating improved accuracy over time. This temporal analysis highlights the LSTM component's ability to adapt to long-term trends, complementing the spatial insights from Figure 8 and informing policy focus on regions with evolving emission patterns.

Table 5. Granular Regional Time-Series Evaluation by MAE Levels

Sector	MAE Range	Sector Avg.	Level 1 Regions	Level 2 Regions	Level 3 Regions	Influential Years	Contextual Notes
Agriculture	0.0004-0.3208	0.0611	North America, Micronesia	Melanesia, Polynesia	East Asia, South Asia	1990, 2001, 2007, 2022	1990: Environmental regulations; 2001: Post-9/11 impact; 2007: Financial crisis effects; 2022: Recovery trends.
Buildings	0.0028-0.2054	0.0539	Melanesia, Polynesia	Micronesia, South Asia	East Asia, Northern Europe	1990, 1999, 2012, 2014	1990: Building codes; 1999: Sustainable design trends; 2012: Policy implementations.

Fuel Exploitation	0.0013-0.4603	0.0660	Micronesia, Melanesia	Polynesia, South Asia	West Asia, East Africa	1991, 1997, 2001, 2015	1991: Gulf War impacts; 1997: Kyoto Protocol discussions; 2015: Paris Agreement.
Industrial Combustion	0.0010-0.3926	0.0570	Northern Europe, Micronesia	Melanesia, West Asia	South Asia, Eastern Europe	1974, 1991, 2014, 2015	1974: Oil crisis; 1991: Regulatory changes; 2015: Global climate actions.
Power Industry	0.0010-0.8188	0.0532	Melanesia, Micronesia	Polynesia, South Asia	East Asia, Northern Europe	1986, 1993, 1995, 2015	1986: Chernobyl disaster; 1993: Energy policy reforms; 2015: Renewables push.
Processes	0.0015-0.8188	0.0467	Melanesia, Micronesia	Polynesia, South Asia	East Asia, West Asia	1974, 1991, 2014, 2015	1974: Industrial regulations; 1991: Environmental standards; 2015: Emission reduction goals.
Transport	0.0067-0.2371	0.0485	Melanesia, North America	Micronesia, Polynesia	South Asia, East Africa	1980, 1990, 1999, 2015	1980: Oil crisis; 1990: Regulatory shifts; 2015: Sustainable transport initiatives.
Waste	0.0010-0.2423	0.0370	Melanesia, Micronesia	Polynesia, South Asia	East Asia, West Asia	1976, 1995, 2015, 2016	1976: Environmental legislation; 1995: Waste management strategies; 2015: Circular economy trends.

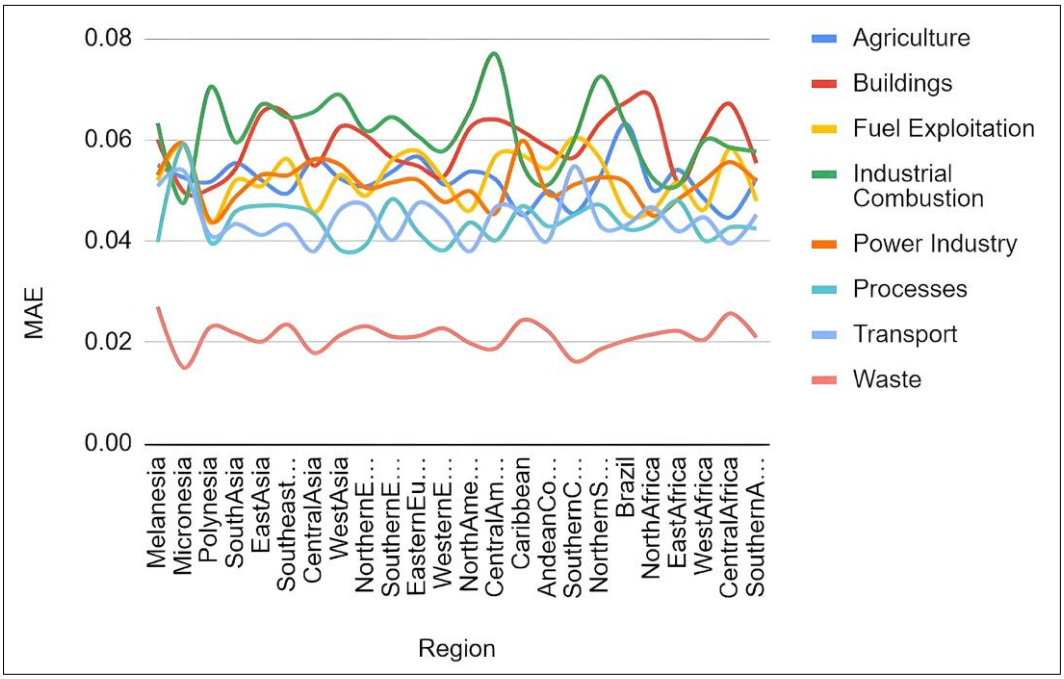

(a) MAE vs. Region

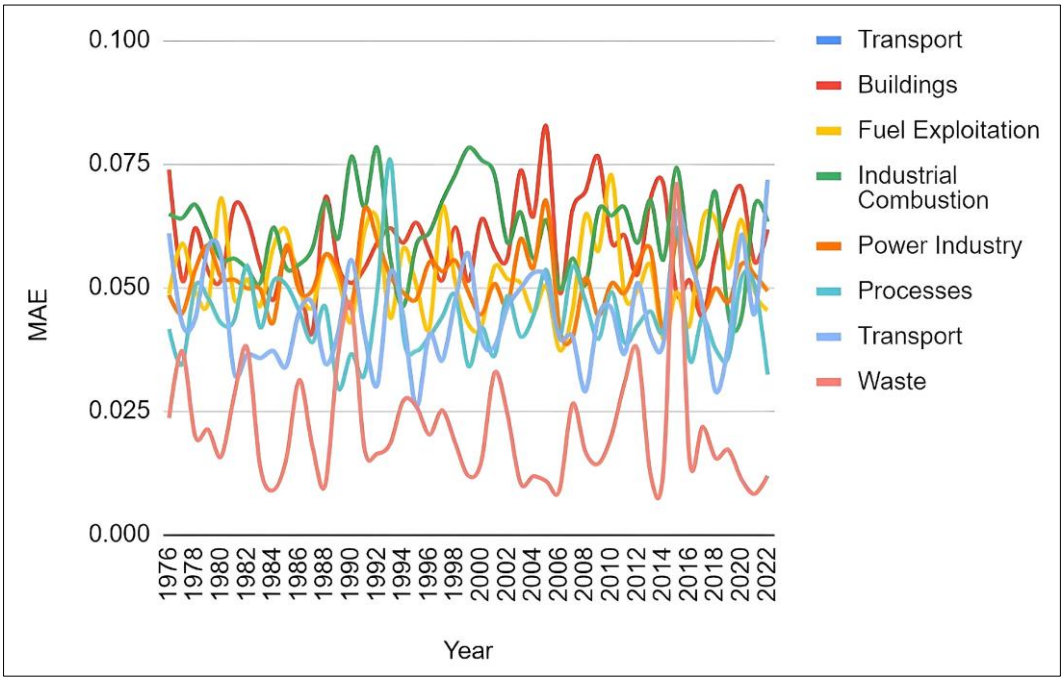

(b) MAE vs Year

Figure 7. Regional Time-Series Evaluation: (a) MAE vs Region and (b) MAE vs Year

(c) Spatial Interpretability: A Case Study of Southeast Asia

Figure 8 captures spatial interpretability, narrowed in scope from 163 countries, 24 clusters, and eight sectors to focus on Southeast Asia as a case study, illustrating the strength of connections between Southeast Asian countries based on geographic proximity and similarities in GHG emissions, as captured by the GCN component of the hybrid GCN-LSTM model. Nodes represent countries annotated by their three-letter country codes (Appendix A), and edges reflect a weighted sum of a 2000 km (Appendix C-1) Haversine geographic proximity and cosine emissions similarity from the adjacency matrix (Section 2-2(b)), filtered at a 0.01 edge strength threshold (Appendix C-2). Across the eight sectors (Appendix A), the model identifies a total of 546 sector-specific connections, comprising 40 unique connections, with 31 above the threshold. Edge colors and thicknesses indicate connection strength: dark blue (<0.0156), sky blue (0.0156–0.0194), orange (0.0194–0.0232), and dark red (>0.0232). For example, the Thailand–Cambodia Waste sector link (brown) exemplifies a strong regional interdependency, driving the level 1 performance observed in Figure 6. This spatial analysis, foundational to the regional robustness in Figure 6 and temporal trends in Figure 7, provides actionable insights for targeted policy cooperation, such as joint waste management strategies between strongly connected countries.

Figure 9 synthesizes the analysis by comparing aggregated time series of actual versus predicted emissions for all eight sectors (Appendix A) and models (GCN-LSTM, ARIMA, Simple LSTM, Stacked LSTM) from 1970 to 2022, as referenced in Section 3-2 (Overall Results for All Four Models). Both Simple and Stacked-LSTM were combined into LSTM for this plot since no visible differences were observed in their plot lines. The vertical axis shows emissions (in $MtCO_2e$). In contrast, the horizontal axis denotes years, with solid blue vertical lines for actual data and wiggly colored lines for predictions (GCN-LSTM: Red, LSTM: Orange, ARIMA: Green). The plots visualize how the GCN-LSTM slightly outperforms its deep-learning counterparts, LSTM and the statistical ARIMA, by more closely aligning with actual emissions for most sectors, reflecting the combined strengths of spatial (Figure 8) and temporal (Figure 7) modeling. This figure confirms the model's reliability for long-term forecasting, offering a comprehensive basis for global climate policy strategies.

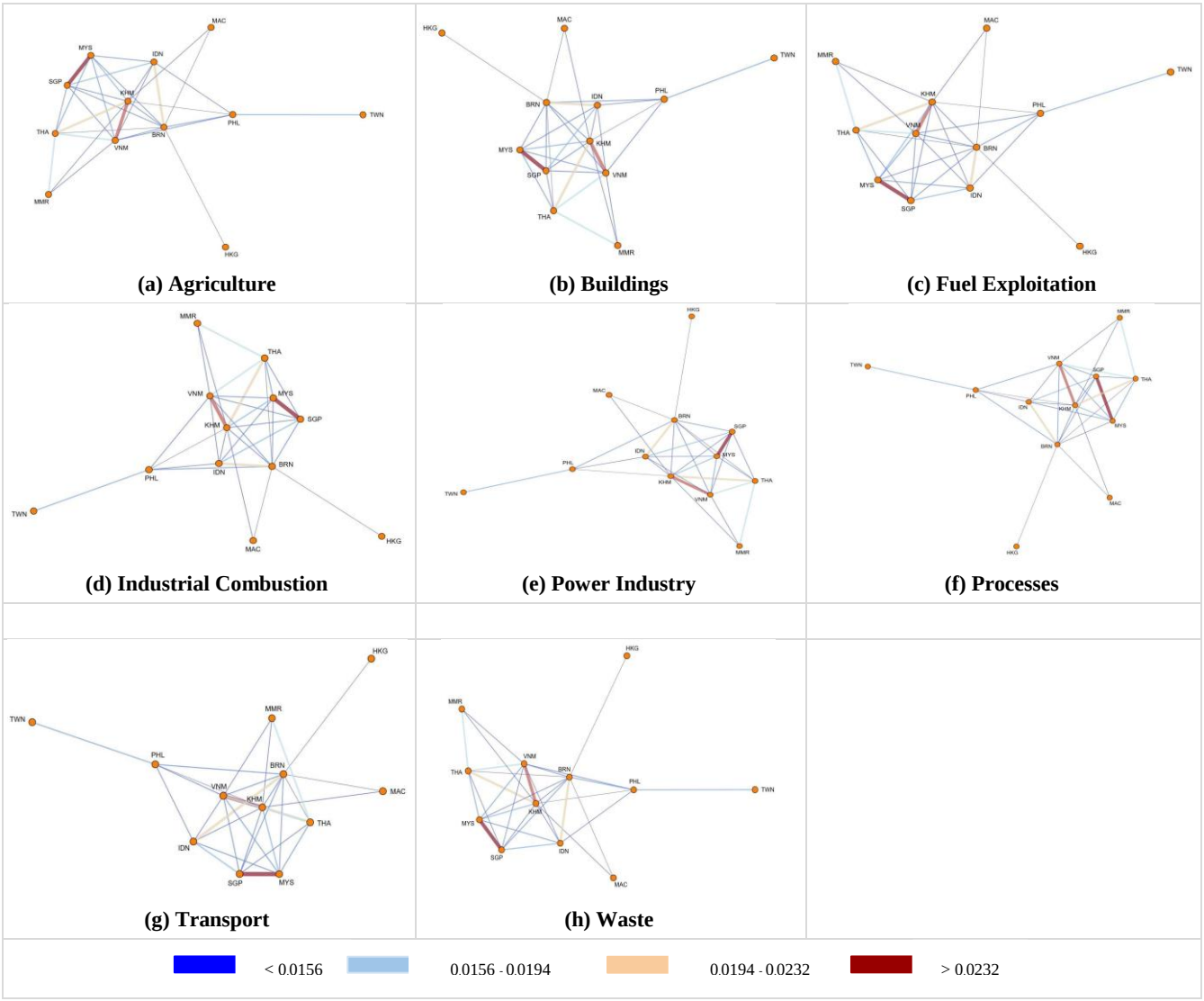

Figure 8. Spatial interpretability by Connection strength with a 0.01 threshold in Southeast Asia

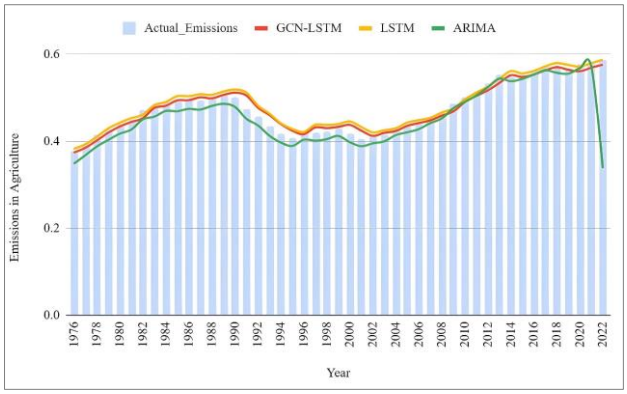

(a) Agriculture

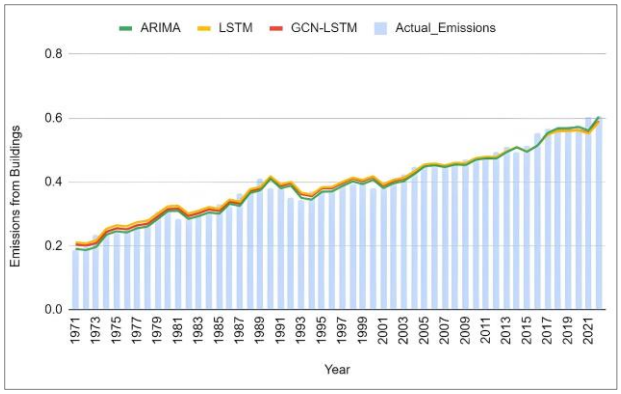

(b) Buildings

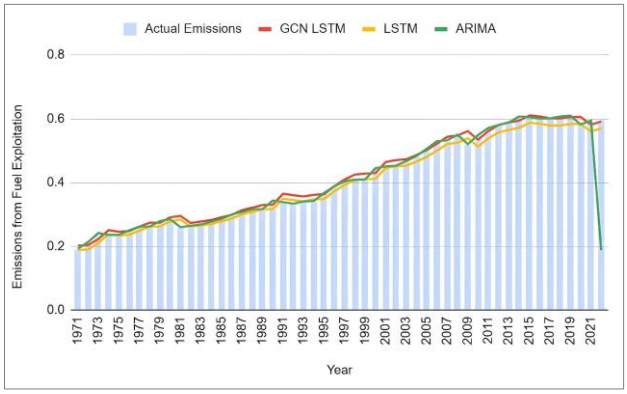

(c) Fuel Exploitation

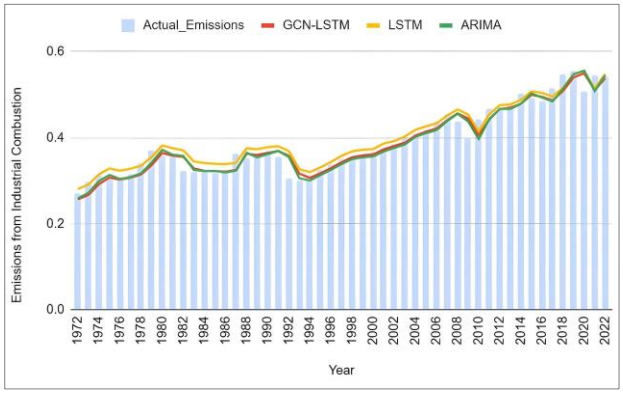

(d) Industrial Combustion

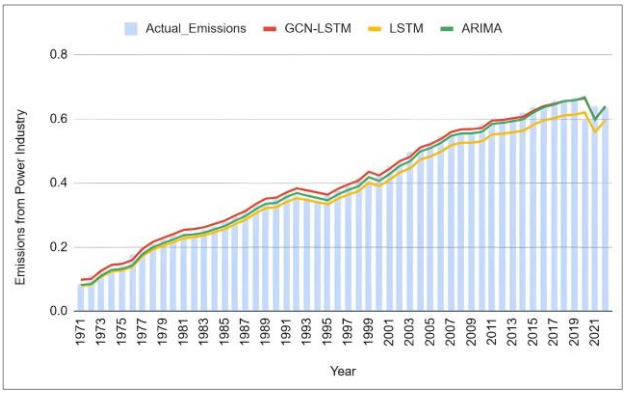

(e) Power Industry

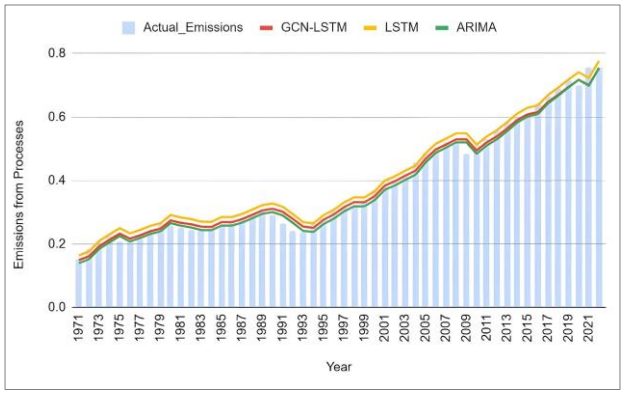

(f) Processes

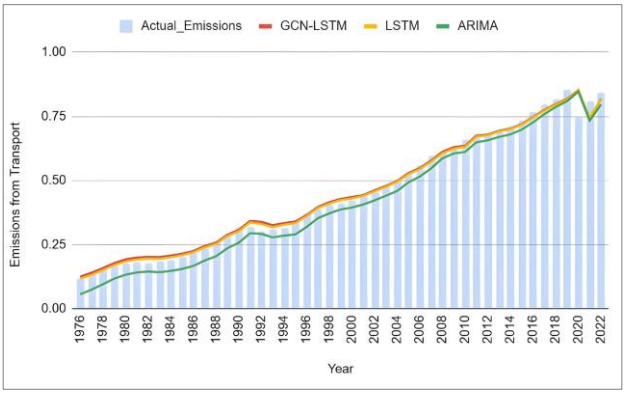

(g) Transport

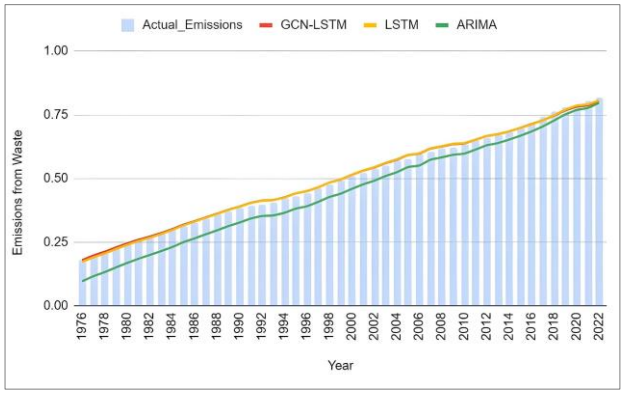

(h) Waste

Figure 9. Aggregated Comparative Time-Series Average Actual vs. Predicted Emissions for All Sectors and All Models

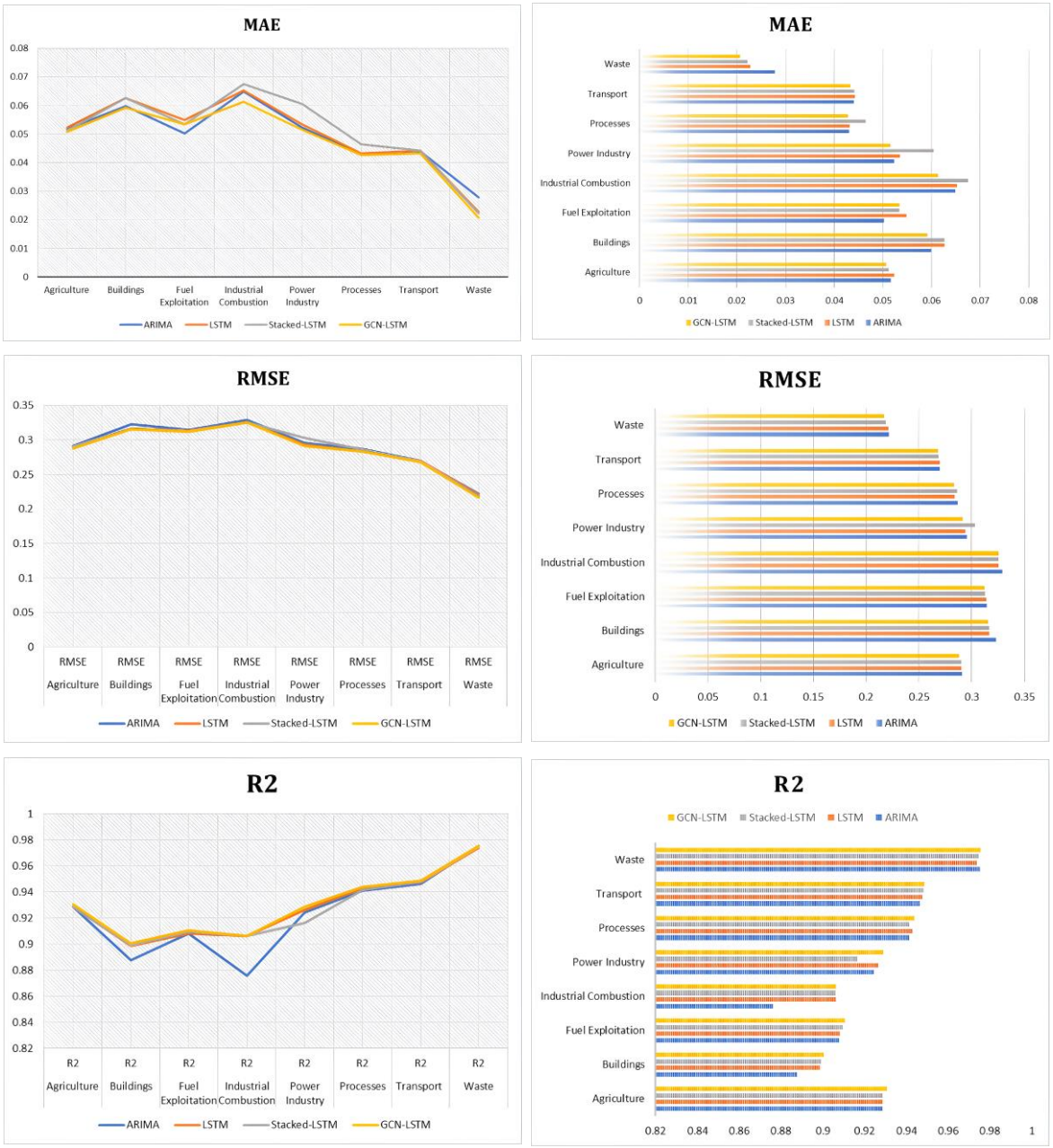

Figure 10. All Models MAE, RMSE, and R^2 Comparison Across All Eight Sectors

3-2- Overall Results for All Four Models

Table 6. All Models' overall performance classification by MAE, RMSE, and R^2 levels

Sectors	Agriculture			Buildings			Fuel Exploitation			Industrial Combustion		
Models	MAE	RMSE	R^2	MAE	RMSE	R^2	MAE	RMSE	R^2	MAE	RMSE	R^2
ARIMA	0.0517	0.2912	0.9288	0.0599	0.3231	0.8876	**0.0502**	0.3144	0.9080	0.0649	0.3293	0.8760
LSTM	0.0523	0.2902	0.9287	0.0627	0.3170	0.8988	0.0549	0.3141	0.9083	0.0652	0.3253	0.9063
Stacked-LSTM	0.0512	0.2903	0.9287	0.0627	0.3166	0.8994	0.0534	0.3128	0.9098	0.0675	0.3256	0.9061
GCN-LSTM	**0.0507**	**0.2882**	**0.9307**	**0.0592**	**0.3158**	**0.9004**	0.0534	**0.3120**	**0.9107**	**0.0614**	**0.3253**	**0.9064**

Sectors	Power Industry			Processes			Transport			Waste		
Models	MAE	RMSE	R^2	MAE	RMSE	R^2	MAE	RMSE	R^2	MAE	RMSE	R^2
ARIMA	0.0523	0.2955	0.9246	0.0431	0.2867	0.9413	0.0441	0.2699	0.9465	0.0279	0.2219	0.9753
LSTM	0.0535	0.2937	0.9265	0.0432	0.2838	0.9428	0.0443	0.2697	0.9476	0.0228	0.2209	0.9738
Stacked-LSTM	0.0605	0.3033	0.9164	0.0465	0.2865	0.9415	0.0442	0.2686	0.9484	0.0222	0.2189	0.9748
GCN-LSTM	**0.0515**	**0.2913**	**0.9289**	**0.0428**	**0.2835**	**0.9439**	**0.0433**	**0.2681**	**0.9487**	**0.0207**	**0.2172**	**0.9756**

3-3- Model Performance by Sector

Building on Figure 9, Figure 10 visualizes the overarching performance metrics of the GCN-LSTM model against ARIMA, Simple LSTM, and Stacked LSTM across the eight sectors (Appendix A), as detailed in Section 3-2 (Overall Results for All Four Models). The figure presents three key metrics: Mean Absolute Error (MAE) in $MtCO_2e$, Root Mean Squared Error (RMSE) in $MtCO_2e$, and Coefficient of Determination (R^2), each displayed with two complementary plots: a line plot and a horizontal bar plot of the same data. For MAE, the line plot traces performance trends across sectors for each model, while the horizontal bar plot reinforces this by showing relative magnitudes. Similarly, RMSE and R^2 follow this dual representation to enhance clarity by combining the line plot's trend visibility with the bar plot's magnitude emphasis.

As seen in Table 6, the GCN-LSTM model outperforms ARIMA, Simple LSTM, and Stacked LSTM across all eight sectors. In the Processes sector, GCN-LSTM achieves a Mean Absolute Error (MAE) of 0.0428 $MtCO_2e$ and a Coefficient of Determination (R^2) of 0.9439, compared to ARIMA's MAE of 0.0467 $MtCO_2e$ and R^2 of 0.9367. Similarly, in the Waste sector, GCN-LSTM records an MAE of 0.0207 $MtCO_2e$ and an R^2 of 0.9756, and in Agriculture, an MAE of 0.0356 $MtCO_2e$. Paired *t*-tests (Appendix B) confirm statistically significant improvements over ARIMA for all sectors, with p-values ($p < 0.05$ for all industries) ranging from 3.80E-07 (Agriculture) to 1.72E-36 (Waste). This aligns with Figure 9's aggregated time series, showing GCN-LSTM closely tracking actual emissions from 1970 to 2022, particularly post-2010. These results highlight the model's ability to capture spatial and temporal dependencies in GHG emissions data, with detailed interpretations provided in Section 4.

4- Discussion

4-1- Overall Comparative Model Performance

The comparative analysis of GCN-LSTM, Simple LSTM, Stacked-LSTM, and ARIMA models across eight distinct sectors (Appendix A) for the key metrics in this study revealed compelling insights into their forecasting capabilities for greenhouse gas emissions. A key observation indicated that deep learning models, including the GCN-LSTM, Simple LSTM, and Stacked-LSTM, consistently outperformed the statistical ARIMA model, as shown in Table 6, section 3-2. Furthermore, comparing the deep learning models independently showed that the GCN-LSTM hybrid model marginally outperformed the others across all sectors, suggesting that incorporating spatial dependencies in time series forecasting of GHG emissions enhanced predictive accuracy [21, 33]. Also, the GCN-LSTM model's statistically significant performance ($p < 0.05$ for all sectors; Appendix B) over the ARIMA model projects the limitations of ARIMA in capturing both non-linear and spatial dependences in emissions data and underscores the GCN-LSTM's potential for precise GHG emissions forecasting, primarily due to its integration of graph convolutional networks (GCNs) to capture inter-country spill-over emissions. For instance, the exceptionally low p-value in Waste ($p = 1.72E-36$) suggests high accuracy, enabling targeted interventions like recycling programs or waste-to-energy initiatives [31]. In Transport, a slightly higher p-value ($p = 3.32E-10$) reflects challenges from volatile fuel use and points to policies like electric vehicle adoption [34]. In Agriculture, the model's accuracy ($p = 3.80E-07$) benefits from spatial features capturing geographic regional similarities and shared economic and agricultural practices [35, 36]. Spatial interpretability, further explained in section 4-3, enhances these findings, revealing strong regional connections, such as Thailand–Cambodia in Waste, which can guide coordinated policies like joint waste management initiatives [37] and pollution remediation [38]. These insights position GCN-LSTM as a powerful tool for creating effective sector-specific climate mitigation strategies.

4-2- Comparison with Previous Studies

When compared to other studies. Yao et al. [11] reported an average R^2 of 0.89 for deep learning models, while our GCN-LSTM achieves a higher average R^2 of 0.93, driven by GCN capturing spatial dependencies absent in their models. Even with spatial dependences and a slightly better R^2 of 0.9661 using a CNN-LSTM, Han et al. [20] recorded a much higher MAE of 8.0169 and RMSE of 11.1505 compared to the GCN-LSTM's MAE of 0.0515, RMSE of 0.2913 in the power and energy industry, suggesting that GCNs are a better fit compared to CNNs at capturing spatial dependences. Wen et al. [39] achieved an MAE of 0.05 $MtCO_2e$ in Transport using an ARIMA-LSTM hybrid, a value 22% higher than the GCN-LSTM's 0.0433. In Agriculture, our model's performance is competitive with traditional methods [5], leveraging GHG per capita data for granular accuracy. The spatial interpretability, aligning with the results of Shao et al. [7], highlights connections like Malaysia–Singapore in Transport, encouraging joint regional policy coordination in this sector [37]. The EDGAR 2023 report of a 1.4% global emission increase [40] corroborates our aggregated trends, although it lacks sectoral granularity, as our model provides precise policy guidance. Despite these positives, challenges remain, such as in the Power Industry, where uneven energy generation and distribution practices, coupled with emission upsets from limited renewable energy adoption, affect emission data [6], suggesting the need for future integration of socioeconomic variables [41].

4-3- Model's Spatial Interpretability: A Case Study of Southeast Asia

To better understand the spatial dependencies, we conducted a spatial interpretability analysis, using Southeast Asia as a case study, as visualized in Figure 8. This analysis revealed that countries sharing geographic borders tended to exhibit stronger connections in terms of GHG emissions. However, proximity to the border alone did not fully explain

the variation in connection strength. For example, in the waste sector, Thailand (THA) shares borders with Cambodia (KHM) and Malaysia (MYS), yet the THA-KHM connection was significantly stronger than the THA-MYS connection. Similarly, the KHM-Vietnam (VNM) connection surpassed KHM-THA in strength. This pattern, consistent across sectors, suggests that factors beyond mere border proximity, such as economic ties, trade relationships, or shared environmental policies, likely influence the strength of emission connections. For instance, the strong connection between Malaysia (MYS) and Singapore (SGP) in the transportation sector can be attributed to their high levels of cross-border trade and travel, as highlighted by studies on cross-border transportation investments in Southeast Asia [42]. Similarly, we found a strong connection between Indonesia (IDN) and Malaysia (MYS) in the power sector, aligning with discussions about regional energy infrastructure and ASEAN's readiness for multilateral electricity trade [37]. In the agriculture sector, the Philippines (PHL) and Indonesia (IDN) exhibited a strong connection, likely due to shared agricultural practices and trade in farm products, as noted in studies on regional agricultural cooperation [43]. This analysis highlights the complexity of inter-country GHG emission relationships in Southeast Asia, with border characteristics, sector-specific activities, and regional collaboration potentially playing significant roles. With such compelling insights, this spatial interpretability serves as a strong indicator of the need for joint regional efforts to mitigate climate change in Southeast Asia. Climate policies with hopes of maximum impact should consider close regional collaboration on waste management and recycling, agricultural land and technology exploitation, transportation infrastructure design, and energy generation and distribution. These actions, fully implemented, could keep the entire region in sync with its mutual emission reduction targets. Future research could explore the impact of border length, economic integration, and policy alignment on these connections to better understand the drivers of emission similarities in the region.

5- Conclusion

This study developed a novel hybrid Graph Convolutional Network–Long Short-Term Memory (GCN-LSTM) model to forecast greenhouse gas (GHG) emissions across 163 countries and eight sectors (Agriculture, Buildings, Fuel Exploitation, Industrial Combustion, Power Industry, Processes, Transport, Waste) using the EDGAR v8 dataset (1970–2022). The model integrates spatial relationships, captured through an adjacency matrix based on geographic proximity and emission similarities, with temporal dynamics modeled by LSTM, achieving superior performance over baseline models (ARIMA, simple LSTM, stacked LSTM). Evaluation metrics, including Mean Absolute Error (MAE: 0.0207 in Waste), Root Mean Squared Error, and Coefficient of Determination (R^2: 0.9756 in Waste), demonstrate the model's high accuracy, validated by 5-fold cross-validation and paired t-tests ($p < 0.05$). Spatial interpretability analysis, complementing the performance metrics, revealed strong regional connections in most sectors, such as Thailand–Cambodia, Malaysia-Singapore, and Cambodia-Vietnam, a powerful endorsement for regional cooperation regarding policy development and action. For example, targeted joint interventions in waste management, recycling, and pollution control practices, including research and development, knowledge exchange, and joint action targets, could contribute substantially to the climate change mitigation strategy in Southeast Asia. The GCN-LSTM model's ability to capture both spatial and temporal dependencies offers a robust framework for multi-country, sector-specific GHG forecasting, addressing limitations of traditional models that overlook spatial correlations and sectoral granularity. This approach provides actionable insights for global climate policy, supporting sustainable development and emission reduction goals. Future work could extend the model to incorporate real-time data and additional socio-economic variables to enhance forecasting precision and further policy relevance. Dynamic re-scaling could also be explored to enable post-2022 data for min-max normalization.

6- Declarations

6-1- Author Contributions

Conceptualization, B.T. and K.J.; methodology, B.T. and K.J.; formal analysis, B.T. and K.J.; investigation, B.T. and K.J.; data curation, B.T. and K.J.; writing—original draft preparation, B.T., K.J., and M.J.; writing—review and editing, B.T., K.J., M.J., and E.S.; project administration, K.J.; funding acquisition, K.J. All authors have read and agreed to the published version of the manuscript.

6-2- Data Availability Statement

(a) Confidential data

The Source Code data presented in this study are available on request from the corresponding author. Due to confidentiality agreements, supporting data can only be made available to bona fide researchers subject to a non-disclosure agreement. Details of the data and how to request access are available from Assoc. Prof. Dr. Krisanadej Jaroensutasinee, PI at the Center of Excellence for Ecoinformatics, Walailak University, Thailand.

(b) Open data

The open datasets analyzed in this study are available in a publicly accessible repository that does not issue DOIs, and can be found here: EDGAR [30]: https://edgar.jrc.ec.europa.eu/dataset_ghg80 (version 8.0) and Simplemaps https://simplemaps.com/resources/free-country-cities (version 1).

6-3- Funding

This work was supported by the Thailand International Cooperation Agency (TICA), Walailak University Graduate Scholarships (No. 02/2024), and the Graduate Research Fund (No. CGS-RF-2025/18) to B. T., the Center of Excellence for Ecoinformatics, Institute of Research and Innovation, Walailak University, and the Government of Cameroon.

6-4- Acknowledgments

This project was conducted within the Reinventing Project for Enhancing Thai Universities into International Education, a project of the Ministry of Higher Education, Science, Research, and Innovation. The authors acknowledge the technical and organizational support provided by the Thailand International Cooperation Agency (TICA), Walailak University, and the Government of Cameroon.

6-5- Institutional Review Board Statement

Not applicable.

6-6- Informed Consent Statement

Not applicable.

6-7- Conflicts of Interest

The authors declare that there is no conflict of interest regarding the publication of this manuscript. In addition, the ethical issues, including plagiarism, informed consent, misconduct, data fabrication and/or falsification, double publication and/or submission, and redundancies have been completely observed by the authors.

7- References

[1] Friedlingstein, P., Jones, M. W., O'Sullivan, M., Andrew, R. M., Bakker, D. C. E., Hauck, J., Le Quéré, C., Peters, G. P., Peters, W., Pongratz, J., Sitch, S., Canadell, J. G., Ciais, P., Jackson, R. B., Alin, S. R., Anthoni, P., Bates, N. R., Becker, M., Bellouin, N., … Zeng, J. (2022). Global Carbon Budget 2021. Earth System Science Data, 14(4), 1917–2005. doi:10.5194/essd-14-1917-2022.

[2] Andrew, R. M. (2018). Global CO_2 emissions from cement production. Earth System Science Data, 10(1), 195–217. doi:10.5194/essd-10-195-2018.

[3] Luo, R., Wang, J., & Gates, I. (2024). Forecasting Methane Data Using Multivariate Long Short-Term Memory Neural Networks. Environmental Modeling and Assessment, 29(3), 441–454. doi:10.1007/s10666-024-09957-x.

[4] Saunois, M., R. Stavert, A., Poulter, B., Bousquet, P., G. Canadell, J., B. Jackson, R., A. Raymond, P., J. Dlugokencky, E., Houweling, S., K. Patra, P., Ciais, P., K. Arora, V., Bastviken, D., Bergamaschi, P., R. Blake, D., Brailsford, G., Bruhwiler, L., M. Carlson, K., Carrol, M., … Zhuang, Q. (2020). The global methane budget 2000-2017. Earth System Science Data, 12(3), 1561–1623. doi:10.5194/essd-12-1561-2020.

[5] Tian, H., Xu, R., Canadell, J. G., Thompson, R. L., Winiwarter, W., Suntharalingam, P., Davidson, E. A., Ciais, P., Jackson, R. B., Janssens-Maenhout, G., Prather, M. J., Regnier, P., Pan, N., Pan, S., Peters, G. P., Shi, H., Tubiello, F. N., Zaehle, S., Zhou, F., … Yao, Y. (2020). A comprehensive quantification of global nitrous oxide sources and sinks. Nature, 586(7828), 248–256. doi:10.1038/s41586-020-2780-0.

[6] Purohit, P., Höglund-Isaksson, L., Dulac, J., Shah, N., Wei, M., Rafaj, P., & Schöpp, W. (2020). Electricity savings and greenhouse gas emission reductions from global phase-down of hydrofluorocarbons. Atmospheric Chemistry and Physics, 20(19), 11305–11327. doi:10.5194/acp-20-11305-2020.

[7] Shao, Z., Gao, S., Zhou, K., & Yang, S. (2024). A new multiregional carbon emissions forecasting model based on a multivariable information fusion mechanism and hybrid spatiotemporal graph convolution network. Journal of Environmental Management, 352, 119976. doi:10.1016/j.jenvman.2023.119976.

[8] Osobajo, O. A., Otitoju, A., Otitoju, M. A., & Oke, A. (2020). The impact of energy consumption and economic growth on carbon dioxide emissions. Sustainability (Switzerland), 12(19), 7965. doi:10.3390/SU12197965.

[9] Wei, S., Wang, T., & Li, Y. (2017). Influencing factors and prediction of carbon dioxide emissions using factor analysis and optimized least squares support vector machine. Environmental Engineering Research, 22(2), 175–185. doi:10.4491/eer.2016.125.

[10] Chukwunonso, B. P., AL-Wesabi, I., Shixiang, L., AlSharabi, K., Al-Shamma'a, A. A., Farh, H. M. H., Saeed, F., Kandil, T., & Al-Shaalan, A. M. (2024). Predicting carbon dioxide emissions in the United States of America using machine learning algorithms. Environmental Science and Pollution Research, 31(23), 33685–33707. doi:10.1007/s11356-024-33460-1.

[11] Yao, X., Zhang, H., Wang, X., Jiang, Y., Zhang, Y., & Na, X. (2024). Which model is more efficient in carbon emission prediction research? A comparative study of deep learning models, machine learning models, and econometric models. Environmental Science and Pollution Research, 31(13), 19500–19515. doi:10.1007/s11356-024-32083-w.

[12] Agarwal, H., Mahajan, G., Shrotriya, A., & Shekhawat, D. (2024). Predictive Data Analysis: Leveraging RNN and LSTM Techniques for Time Series Dataset. Procedia Computer Science, 235, 979–989. doi:10.1016/j.procs.2024.04.093.

[13] Crespo-Otero, A., Esteve, P., & Zanin, M. (2024). Deep Learning models for the analysis of time series: A practical introduction for the statistical physics practitioner. Chaos, Solitons and Fractals, 187, 115359. doi:10.1016/j.chaos.2024.115359.

[14] Roy, D. S. (2020). Forecasting the Air Temperature at a Weather Station Using Deep Neural Networks. Procedia Computer Science, 178, 38–46. doi:10.1016/j.procs.2020.11.005.

[15] Boubaker, S., Benghanem, M., Mellit, A., Lefza, A., Kahouli, O., & Kolsi, L. (2021). Deep Neural Networks for Predicting Solar Radiation at Hail Region, Saudi Arabia. IEEE Access, 9, 36719–36729. doi:10.1109/ACCESS.2021.3062205.

[16] Hamdan, A., Al-Salaymeh, A., AlHamad, I. M., Ikemba, S., & Ewim, D. R. E. (2023). Predicting future global temperature and greenhouse gas emissions via LSTM model. Sustainable Energy Research, 10(1), 21. doi:10.1186/s40807-023-00092-x.

[17] Sha, M., Emmanuel, S., Bindhu, A., & Mustaq, M. (2024). Intensified greenhouse gas prediction: Configuring Gate with Fine-Tuning Shifts with Bi-LSTM and GRU System. Frontiers in Climate, 6, 1457441. doi:10.3389/fclim.2024.1457441.

[18] García-Duarte, L., Cifuentes, J., & Marulanda, G. (2023). Short-term spatio-temporal forecasting of air temperatures using deep graph convolutional neural networks. Stochastic Environmental Research and Risk Assessment, 37(5), 1649–1667. doi:10.1007/s00477-022-02358-0.

[19] Waqas, M., & Humphries, U. W. (2024). A critical review of RNN and LSTM variants in hydrological time series predictions. MethodsX, 13, 102946. doi:10.1016/j.mex.2024.102946.

[20] Han, Z., Cui, B., Xu, L., Wang, J., & Guo, Z. (2023). Coupling LSTM and CNN Neural Networks for Accurate Carbon Emission Prediction in 30 Chinese Provinces. Sustainability (Switzerland), 15(18), 13934. doi:10.3390/su151813934.

[21] Azzam, A., Sanami, S., & Aghdam, A. G. (2024). Load Forecasting using GNN-LSTM Attention Mechanism with Low-Frequency Data. Proceedings of SysCon 2024 - 18th Annual IEEE International Systems Conference, 1–6. doi:10.1109/SysCon61195.2024.10553600.

[22] Zhang, X., & Wang, D. (2023). A GNN-based Day Ahead Carbon Intensity Forecasting Model for Cross-Border Power Grids. E-Energy 2023 - Proceedings of the 2023 14th ACM International Conference on Future Energy Systems, 361–373. doi:10.1145/3575813.3597346.

[23] Liao, W., Yang, D., Wang, Y., & Ren, X. (2021). Fault diagnosis of power transformers using graph convolutional network. CSEE Journal of Power and Energy Systems, 7(2), 241–249. doi:10.17775/CSEEJPES.2020.04120.

[24] Huang, D., Liu, H., Bi, T., & Yang, Q. (2022). GCN-LSTM spatiotemporal-network-based method for post-disturbance frequency prediction of power systems. Global Energy Interconnection, 5(1), 96–107. doi:10.1016/j.gloei.2022.04.008.

[25] Chen, H., Zhu, M., Hu, X., Wang, J., Sun, Y., Yang, J., Li, B., & Meng, X. (2023). Multifeature Short-Term Power Load Forecasting Based on GCN-LSTM. International Transactions on Electrical Energy Systems, 2023, 8846554. doi:10.1155/2023/8846554.

[26] Azati, Y., Wang, X., Quddus, M., & Zhang, X. (2025). Graph convolutional LSTM algorithm for real-time crash prediction on mountainous freeways. International Journal of Transportation Science and Technology, 18(3), 272–284. doi:10.1016/j.ijtst.2024.07.002.

[27] Li, P., Zhang, T., & Jin, Y. (2023). A Spatio-Temporal Graph Convolutional Network for Air Quality Prediction. Sustainability (Switzerland), 15(9), 7624. doi:10.3390/su15097624.

[28] Friedlingstein, P., O'Sullivan, M., Jones, M. W., Andrew, R. M., Bakker, D. C. E., Hauck, J., Landschützer, P., Le Quéré, C., Luijkx, I. T., Peters, G. P., Peters, W., Pongratz, J., Schwingshackl, C., Sitch, S., Canadell, J. G., Ciais, P., Jackson, R. B., Alin, S. R., Anthoni, P., … Zheng, B. (2023). Global Carbon Budget 2023. Earth System Science Data, 15(12), 5301–5369. doi:10.5194/essd-15-5301-2023.

[29] Chen, C., Guo, J., Zhang, L., Wu, X., & Yang, Z. (2024). Robust multi-scale time series prediction for building carbon emissions with explainable deep learning. Energy and Buildings, 312, 114159. doi:10.1016/j.enbuild.2024.114159.

[30] Pfenning-Butterworth, A., Buckley, L. B., Drake, J. M., Farner, J. E., Farrell, M. J., Gehman, A. L. M., Mordecai, E. A., Stephens, P. R., Gittleman, J. L., & Davies, T. J. (2024). Interconnecting global threats: climate change, biodiversity loss, and infectious diseases. The Lancet Planetary Health, 8(4), e270–e283. doi:10.1016/S2542-5196(24)00021-4.

[31] Stefănescu, C. A., Dobrea, R. C., & Loghin, M. (2022). A Comparative Analysis of Waste Management Systems Used for Environmental Protection: Norway (Oslo) – Zanzibar (Zanzibar). Proceedings of the International Management Conference, 15(1), 195–205. doi:10.24818/Imc/2021/01.19.

[32] Dash, C. S. K., Behera, A. K., Dehuri, S., & Ghosh, A. (2023). An outliers detection and elimination framework in classification task of data mining. Decision Analytics Journal, 6, 100164. doi:10.1016/j.dajour.2023.100164.

[33] Pan, F., Yang, Y., Ji, Y., Li, J., Zhang, J., & Zhong, L. (2024). Application of improved graph convolutional networks in daily-ahead carbon emission prediction. Frontiers in Energy Research, 12, 1371507. doi:10.3389/fenrg.2024.1371507.

[34] Jelti, F., Allouhi, A., & Tabet Aoul, K. A. (2023). Transition Paths towards a Sustainable Transportation System: A Literature Review. Sustainability (Switzerland), 15(21), 15457. doi:10.3390/su152115457.

[35] Yuan, Y., Wang, Y., Chi, Y., & Jin, F. (2020). Identification of key carbon emission sectors and analysis of emission effects in China. Sustainability (Switzerland), 12(20), 1–19. doi:10.3390/su12208673.

[36] Mishra, T., & Nair, P. S. (2024). Advancing Agriculture Predictive Models for Farming Suitability Using Machine Learning. International Journal of Intelligent Systems and Applications in Engineering, 12(5s), 494–502.

[37] Do, T. N., & Burke, P. J. (2023). Is ASEAN ready to move to multilateral cross-border electricity trade? Asia Pacific Viewpoint, 64(1), 110–125. doi:10.1111/apv.12343.

[38] Mele, M., Magazzino, C., Schneider, N., & Nicolai, F. (2021). Revisiting the dynamic interactions between economic growth and environmental pollution in Italy: evidence from a gradient descent algorithm. Environmental Science and Pollution Research, 28(37), 52188–52201. doi:10.1007/s11356-021-14264-z.

[39] Wen, T., Liu, Y., Bai, Y. he, & Liu, H. (2023). Modeling and forecasting CO_2 emissions in China and its regions using a novel ARIMA-LSTM model. Heliyon, 9(11), 21241. doi:10.1016/j.heliyon.2023.e21241.

[40] Crippa, M., Guizzardi, D., Muntean, M., Schaaf, E., Dentener, F., Van Aardenne, J. A., Monni, S., Doering, U., Olivier, J. G. J., Pagliari, V., & Janssens-Maenhout, G. (2018). Gridded emissions of air pollutants for the period 1970-2012 within EDGAR v4.3.2. Earth System Science Data, 10(4), 1987–2013. doi:10.5194/essd-10-1987-2018.

[41] Kumari, S., & Singh, S. K. (2023). Machine learning-based time series models for effective CO_2 emission prediction in India. Environmental Science and Pollution Research, 30(55), 116601–116616. doi:10.1007/s11356-022-21723-8.

[42] ADBI. (2014). Assessing the costs and benefits of economic integration in Southeast Asia. Asian Development Bank Institute, ADBI Working Paper Series, 483. Available online: https://www.adb.org/sites/default/files/publication/156338/adbi-wp483.pdf (accessed on January 2026).

[43] ADB. (2018). Agricultural cooperation in Southeast Asia: Opportunities and challenges. Asian Development Bank, ADB Briefs, 106. doi:10.22617/TCS189598-2.

Appendix A: List of Countries, Substances, Sectors, and Regional Clusters

Countries	Afghanistan, Angola, Argentina, Armenia, Australia, Austria, Azerbaijan, Burundi, Belgium, Burkina Faso, Bangladesh, Bulgaria, Bahamas, Bosnia and Herzegovina, Belarus, Belize, Bolivia, Brazil, Barbados, Brunei, Bhutan, Central African Republic, Canada, Switzerland and Liechtenstein, Chile, China, Côte d'Ivoire, Cameroon, Democratic Republic of the Congo, Colombia, Comoros, Cabo Verde, Costa Rica, Cuba, Cyprus, Czechia, Germany, Djibouti, Dominica, Denmark, Dominican Republic, Algeria, Ecuador, Egypt, Eritrea, Spain and Andorra, Estonia, Ethiopia, Finland, Fiji, France and Monaco, United Kingdom, Georgia, Guinea, Guadeloupe, The Gambia, Guinea-Bissau, Greece, Guatemala, French Guiana, Guyana, Hong Kong, Croatia, Haiti, Hungary, Indonesia, India, Ireland, Iran, Iraq, Israel and Palestine, State of, Italy, San Marino and the Holy See, Jamaica, Jordan, Japan, Kazakhstan, Kenya, Kyrgyzstan, Cambodia, Kiribati, South Korea, Kuwait, Lebanon, Liberia, Libya, Saint Lucia, Sri Lanka, Lesotho, Lithuania, Luxembourg, Latvia, Macao, Morocco, Moldova, Madagascar, Maldives, Mexico, North Macedonia, Mali, Myanmar/Burma, Mongolia, Mozambique, Mauritania, Martinique, Malawi, Malaysia, New Caledonia, Nigeria, Nicaragua, Netherlands, Norway, New Zealand, Oman, Pakistan, Panama, Peru, Philippines, Papua New Guinea, Poland, Puerto Rico, North Korea, Portugal, Qatar, Réunion, Romania, Russia, Saudi Arabia, Serbia and Montenegro, Sudan and South Sudan, Senegal, Singapore, Solomon Islands, Sierra Leone, Somalia, São Tomé and Príncipe, Suriname, Slovakia, Slovenia, Sweden, Seychelles, Syria, Chad, Thailand, Turkmenistan, Tonga, Trinidad and Tobago, Tunisia, Türkiye, Taiwan, Tanzania, Uganda, Ukraine, Uruguay, United States, Uzbekistan, Saint Vincent and the Grenadines, Venezuela, Vietnam, Vanuatu, Samoa, South Africa, Zambia, Zimbabwe
Substances	CO2, GWP_100_AR5_CH4, GWP_100_AR5_N20, GWP_100_AR5_F-Gases
Sectors	**Agriculture**: Emissions from agricultural activities such as livestock, crop cultivation, and agricultural waste management. **Buildings**: Emissions from residential and commercial buildings, including heating, cooling, and cooking. **Fuel Exploitatio**n: Emissions from the extraction and processing of fossil fuels, including coal, oil, and natural gas. **Industrial Combustion**: Emissions from industrial processes that involve combustion, such as manufacturing and power generation. **Power Industry**: Emissions from fossil fuel power plants in electricity generation. **Processes**: Emissions from industrial processes that do not involve combustion, such as chemical production and metal smelting. **Transport**: Emissions from road, rail, air, and marine transportation. **Waste**: Emissions from the disposal of waste, including landfills and waste incineration.
Regional Clusters	**Melanesia:** FJI, PNG, SLB, VUT **Micronesia**: FSM, KIR, MHL, NRU, PLW **Polynesia**: ASM, COK, NIU, PCN, WSM, TON, TUV **East Asia**: CHN, JPN, KOR, MNG, PRK, TWN **South Asia**: AFG, BGD, BTN, IND, LKA, MDV, NPL, PAK **Southeast Asia**: BRN, KHM, IDN, LAO, MMR, MYS, PHL, SGP, THA, TLS, VNM **Central Asia**: KAZ, KGZ, TJK, TKM, UZB **West Asia**: ARM, AZE, BHR, CYP, GEO, IRQ, ISR, JOR, KWT, LBN, OMN, PSE, QAT, SAU, SYR, TUR, ARE, YEM **Northern Europe**: DNK, EST, FIN, ISL, IRL, LTU, LVA, NOR, SWE, GBR **Southern Europe**: ALB, AND, BIH, HRV, GRC, ITA, MLT, MNE, PRT, SMR, ESP, SRB, MKD, VAT **Eastern Europe**: ARM, AZE, BLR, BGR, CZE, GEO, HUN, MDA, POL, ROU, RUS, SVK, SVN, UKR **Western Europe**: AUT, BEL, FRA, DEU, LIE, LUX, MCO, NLD, CHE **North America**: CAN, USA, MEX **Central America**: BLZ, CRI, SLV, GTM, HND, NIC, PAN **Caribbean**: ATG, BHS, BRB, CUB, DMA, DOM, GRD, HTI, JAM, KNA, LCA, VCT, TTO **Andean Countries**: BOL, COL, ECU, PER, VEN **Southern Cone**: ARG, CHL, PRY, URY **Northern South** America: GUY, SUR **Brazil**: BRA **North Africa**: DZA, EGY, LBY, MAR, SDN, TUN **East Africa**: BDI, COM, DJI, ERI, ETH, KEN, MDG, RWA, SOM, SSD, TZA, UGA **West Africa**: BEN, BFA, CIV, CPV, GHA, GIN, GMB, GNB, LBR, MLI, NER, NGA, SEN, SLE, TGO **Central Africa**: AGO, CAF, CMR, COD, COG, GNQ, GAB, STP, TCD **Southern Africa**: BWA, LSO, NAM, SWZ, ZAF, ZMB, ZWE

Appendix B: Paired T-tests on MAE between GCN-LSTM and ARIMA

Sector	t-statistic	p-value
Agriculture	-5.29639	3.80E-07
Buildings	-2.04324	0.042649
Fuel Exploitation	3.968404	0.000108
Industrial Combustion	-2.88404	0.00446
Power Industry	-3.73902	0.000256
Processes	-4.23047	3.89E-05
Transport	-6.69712	3.32E-10
Waste	-16.4907	1.72E-36

Appendix C: Obtaining 2000 km Threshold distance and 0.01 threshold edge strength

1. 2000 km Threshold Distance

South East Asian countries and their capital cities:

Country Code	Country Name	Capital City	Latitude	Longitude
BRN	Brunei Darussalam	Bandar Seri Begawan	4.9333° N	114.9333° E
KHM	Cambodia	Phnom Penh	11.5500° N	104.9167° E
IDN	Indonesia	Jakarta	6.2088° S	106.8456° E
LAO	Laos	Vientiane	17.9667° N	102.6000° E
MMR	Myanmar	Naypyidaw	19.7633° N	96.0780° E
MYS	Malaysia	Kuala Lumpur	3.1390° N	101.6869° E
PHL	Philippines	Manila	14.5995° N	120.9842° E
SGP	Singapore	Singapore City	1.3521° N	103.8198° E
THA	Thailand	Bangkok	13.7500° N	100.4833° E
TLS	Timor-Leste	Dili	8.5583° S	125.5603° E
VNM	Vietnam	Hanoi	21.0285° N	105.8542° E

Haversine Distance (in km) between Capital Cities:

From \ To	BRN	KHM	IDN	LAO	MMR	MYS	PHL	SGP	THA	TLS	VNM
BRN	-	1184	1381	1675	2056	1211	1195	1083	1445	1761	1526
KHM	1184	-	1888	475	887	862	1461	1022	510	2884	987
IDN	1381	1888	-	2748	2963	1168	2631	1159	2341	2776	2901
LAO	1675	475	2748	-	623	1340	2038	1500	517	3449	992
MMR	2056	887	2963	623	-	1718	2277	1882	832	3647	1118
MYS	1211	862	1168	1340	1718	-	2490	300	1188	2793	1222
PHL	1195	1461	2631	2038	2277	2490	-	2382	1782	2671	1738
SGP	1083	1022	1159	1500	1882	300	2382	-	1162	2749	1104
THA	1445	510	2341	517	832	1188	1782	1162	-	3183	991
TLS	1761	2884	2776	3449	3647	2793	2671	2749	3183	-	3217
VNM	1526	987	2901	992	1118	1222	1738	1104	991	3217	-

Calculation of Average Distance:

There are $N \times (N-1)/2$ unique pairs for N countries. For 11 countries, this is $11 \times 10/2 = 55$ unique pairs.

Total Sum of Distances = 99,697 km

Average Distance = Total Sum / Number of Pairs = 99,697 km / 55

Average Haversine Distance between Capital Cities = 1812.67 km (approximately)

2. 0.01 Threshold Edge Strength for waste sector

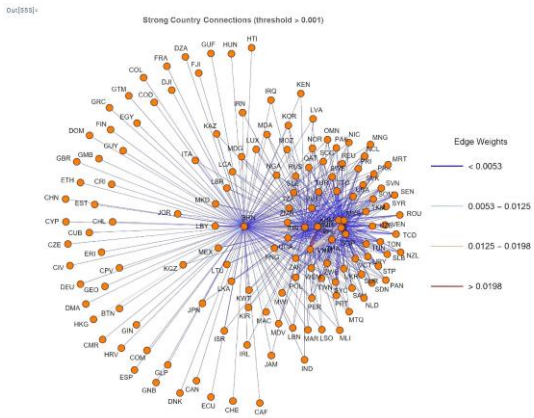

0.001

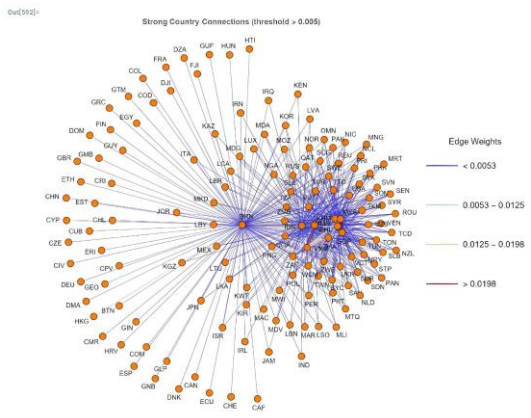

0.005

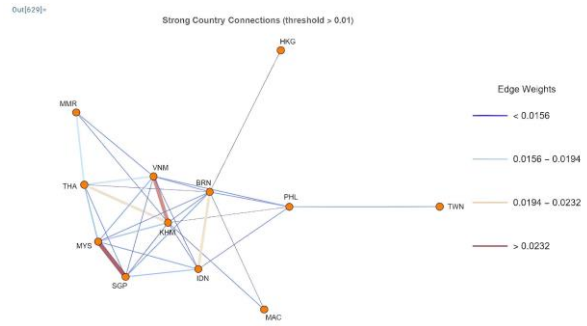

0.01

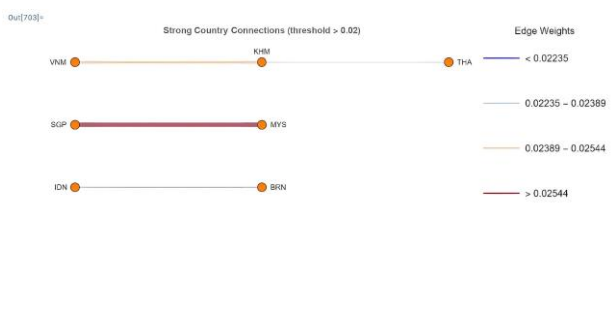

0.02